Instability of aquaglyceroporin (AQP) 2 contributes to drug resistance in *Trypanosoma brucei*

Juan F. Quintana[1], Juan Bueren-Calabuig[1], Fabio Zuccotto[1], Harry P. de Koning[2], David Horn[1], and Mark C. Field[1,3]*

[1]School of Life Sciences, University of Dundee, Dow Street, Dundee DD1 5EH, UK. [2]Institute of Infection, Immunity, and Inflammation, University of Glasgow, Glasgow, UK. [3]Biology Centre, Institute of Parasitology, Biology Centre, Czech Academy of Sciences, Ceske Budejovice, Czech Republic.

Present address: JFQ, Wellcome Centre for Integrative Parasitology, College of Medical, Veterinary and Life Sciences, Glasgow Biomedical Research Centre, University of Glasgow, Glasgow, UK.

*__Corresponding author:__ mfield@mac.com

Running head: Aquaporin trafficking in trypanosomes

Keywords: *Trypanosoma brucei*, aquaglyceroporin, ubiquitylation, protein stability, pentamidine, drug resistance.

Abstract

Defining mode of action is vital for both developing new drugs and predicting potential resistance mechanisms. African trypanosome pentamidine and melarsoprol sensitivity is predominantly mediated by aquaglyceroporin 2 (TbAQP2), a channel associated with water/glycerol transport. TbAQP2 is expressed at the flagellar pocket membrane and chimerisation with TbAQP3 renders parasites resistant to both drugs. Two models for how TbAQP2 mediates pentamidine sensitivity have emerged; that TbAQP2 mediates pentamidine translocation or via binding to TbAQP2, with subsequent endocytosis, but trafficking and regulation of TbAQPs is uncharacterised. We demonstrate that TbAQP2 is organised as a high order complex, is ubiquitylated and transported to the lysosome. Unexpectedly, mutation of potential ubiquitin conjugation sites, i.e. cytoplasmic lysine residues, reduced folding and tetramerization efficiency and triggered ER retention. Moreover, TbAQP2/TbAQP3 chimerisation also leads to impaired oligomerisation, mislocalisation, and increased turnover. These data suggest that TbAQP2 stability is highly sensitive to mutation and contributes towards emergence of drug resistance.

Introduction

Human African trypanosomiasis (HAT) is a neglected tropical disease affecting sub-Saharan countries [1–4]. HAT progresses by two stages: a haemolymphatic stage, in which the parasite successfully colonises the bloodstream, lymphatics, skin, adipose tissue and organs and a meningoencephalic stage characterised by the emergence of parasites in the central nervous system (CNS) [2,5]. Several drugs are used to treat HAT; currently suramin and pentamidine are the drugs of choice for treatment of the haemolymphatic stage of *T. brucei rhodesiense* and *T. brucei gambiense* infections respectively, whereas melarsoprol, eflornithine or combined nifurtimox-eflornithine (NECT) therapy are recommended for the meningoencephalic stage [6,7].

Two new drugs, fexinidazole and acoziborole, recently completed clinical trials and opened a new front in HAT chemotherapy [8,9]. Drug development, successful public health initiatives and active case-monitoring programs have all contributed to the anticipated eradication of *gambiense* HAT as a major public health problem in the coming decade [10]. However, vigilance and understanding of drug mechanisms and possible resistance pathways remain essential to maintain this situation, and *rhodesiense* HAT cannot be eliminated in this way as it is highly zoonotic [11]. Genome-wide RNAi screens identified a number of genes associated with pentamidine sensitivity that, together with evidence from melarsoprol-pentamidine cross-resistance (MPXR), identified aquaglyceroporin 2 as the primary determinant for drug-uptake [12,13], alongside lesser roles for the TbAT1/P2 aminopurine transporter and the Low Affinity Pentamidine transporter LAPT1 [14].

Aquaglyceroporins (AQPs) are an ancient family of multi-pass membrane proteins, containing both aquaporins that exclusively transport water and aquaglyceroporins that transport both water and uncharged low molecular weight solutes [15–17]. The *T. brucei* genome encodes three AQPs (TbAQP1-3) [18], all of which are nonessential but do control osmoregulation and glycerol transport [13,19–24]. TbAQP1 (Tb927.6.1520) and TbAQP2 (Tb927.10.14170) are typically localised to the flagellum and flagellar pocket respectively, whereas TbAQP3 (Tb927.10.14160) is associated with bulk plasma membrane [13,21,23]. TbAQP2 and TbAQP3 are the product of a recent gene duplication within the African trypanosome lineage [13,21,23,25].

A selectivity filter restricts the size and properties of solutes that can effectively pass through the AQP pore [15–17]. In TbAQP1 and TbAQP3, this is formed by two constrictions of the channel: the canonical "NPA" within two half alpha helices and a narrower "aromatic/Arginine" (ar/R) motif (Fig. 1A) [13,25,26]. Significantly, TbAQP2 does not retain the canonical configuration but displays an unconventional "NPS/NSA" cation filter motif. Similarly, the ar/R motif is replaced by a neutral leucine at position 264 (L264), followed by aliphatic rather than aromatic residues (A88, I110, V249 and L258), which are equivalent to the "IVLL" motif observed in the selectivity pore of other AQPs [13,23]. These substitutions may permit TbAQP2 to transport larger solutes, including pentamidine (340 Da) [23]. However, pentamidine also binds TbAQP2 with nanomolar affinity and replacement of the Leucine 264 by arginine abolishes binding, leading to resistance [22], consistent with a proposed hypothesis that pentamidine sensitivity might be mediated by high affinity binding of pentamidine to TbAQP2 and internalisation *via* endocytosis [22]. It is also plausible that pentamidine exploits both channel activity and endocytosis of TbAQP2 to gain entry to the trypanosome cytoplasm.

Melarsoprol-pentamidine cross-resistant strains and field isolates from relapse patients all possess mutations at the locus encoding TbAQP2, including deletions, single nucleotide polymorphisms and chimerisation [27–30]. Pentamidine-resistant trypanosomes from a cohort of relapse patients from the Democratic Republic of Congo also have TbAQP2 chimerisation with the coding sequence for the C-terminal *trans*-membrane domain replaced by TbAQP3 and in most cases without altering the selectivity filter characteristic of TbAQP2 (NSA/NPS – IVLL motifs) [29,31,32]. These observations indicate that, in addition to the sequence at the selectivity pore, other features are likely to impact drug uptake and transport in *T. brucei* [33].

Here, we set out to investigate TbAQP2 trafficking and to understand the basis of drug resistance in chimeras where the selectivity filter remains intact. We find that AQPs form a tetramer of tetramers (4x4) quaternary structure which correlates with high stability, flagellar pocket localisation and functionality. Furthermore, we demonstrate that TbAQP2 is ubiquitylated and highly sensitive to mutation of cytoplasmically oriented lysine residues. Finally, we find that chimerisation of TbAQP2, as observed in DRC patients, leads to protein instability and mislocalisation, thus explaining the basis for drug resistance in clinical isolates of *T. brucei*.

Materials and methods

Cell culture and drug sensitivity

Bloodstream form (BSF) *T. brucei* 2T1 and all derivatives were cultured in HMI-11 (supplemented with 10% heat-inactivated fetal bovine serum (FBS), 100 U/ml penicillin, 100 U/ml streptomycin and 2 mM L-glutamine) at 37˚C with 5% CO_2 in a humid atmosphere in non-adherent culture flasks with vented caps at densities between 1 x 10^5 and 1.5 x 10^6 cells/ml. 2T1 cells were maintained in the presence of phleomycin (1 µg/ml) and puromycin (1 µg/ml). Following transformation, cells were selected and maintained with hygromycin (2.5 µg/ml) or phleomycin (1 µg/ml) as appropriate. EC_{50} determinations were performed using AlamarBlue® (resazurin sodium salt) as described [34,35], with 5 mM glycerol added as appropriate; drug exposure was for 66 hours and AlamarBlue® incubation overnight. Plates were read on an Infinite 200Pro plate-reader (Tecan) with the following parameters: excitation, 530nm; emission 585 nm; filter cut-off, 570 nm. Proliferation was monitored by dilution to 1 x 10^5 cells/ml and counting daily. For transfections, 3 x 10^7 bloodstream form cells were harvested by centrifugation and transfected with 5-10 µg of linearized plasmid DNA using an Amaxa Nucleofector II (Lonza) with program X-001. Bafilomycin A1, MG132, Salicylhydroxamic acid (SHAM), glycerol, AlamarBlue®, pentamidine and ammonium chloride were all from Sigma.

Recombinant DNA manipulation

To express N- or C-terminal HA-tagged AQP constructs, a tandem of three HA tags was inserted by PCR using the primers: Tb^{3xHA}_AQP2_Fwd (HindIII): CCCAAGCTTGGGATGTACCCATACGATGTTCCAGATTACGCTTACCCATACGAT GTTCCAGATTACGCTTACCCATACGATGTTCCAGATTACGCTCAGAGCCAACCA GACAATGTG and Tb^{3xHA}_AQP2_Rev (BamHI): CGCGGATCCGCGTTAGTGTGGAAGAAAATATTTGTAC. The PCR products were inserted into $pRPa^{TAG}$ [12] after digestion with BamHI/HindIII. All constructs were verified by sequencing (MRC-PPU DNA Sequencing facility, University of Dundee). Prior to introduction into trypanosomes $pRPa^{TAG}$ constructs were linearized with AscI and purified/sterilized by phenol:chloroform extraction. TbAQP2, with all lysine residues predicted facing the cytoplasm mutated ($TbAQP2^{5K>R}$) was designed and synthesized by GenScript and verified by sequencing. Point mutations rescuing individual lysine residues were introduced using the Q5 Site-Directed Mutagenesis Kit

(NEB) and confirmed by sequencing. Tagging of lysine mutants was conducted as above.

Imaging

Antibodies were used at the following dilutions: rat anti-HA IgG_1 (clone 3F10; Sigma) at 1:1000, rabbit anti-ISG75 (in house) at 1:500, mouse anti-p67 (from J. Bangs) at 1:500. Secondary antibodies (Thermo) were at: anti-rat Alexa-568 at 1:1,000, anti-rabbit Alexa-488 at 1: 1,000, anti-mouse Alexa-488 at 1: 1,000. Coverslips were mounted using Vectashield mounting medium supplemented with 1 ug/ml 4,6-diamidino-2-phenylindole (DAPI; Vector Laboratories, Inc.). Slides were examined on a Zeiss Axiovert 200 microscope with an AxioCam camera and ZEN Pro software (Carl Zeiss, Germany). For co-localization cells were analysed by confocal microscopy with a Leica TCS SP8 confocal laser scanning microscope and the Leica Application Suite X (LASX) software (Leica, Germany). Images were acquired as *z*-stacks (0.25 μm). Digital images were processed using the Omero Open microscopy environment (University of Dundee; https://www.openmicroscopy.org/omero/). In all cases, images for a specific analysis were acquired with identical settings.

Protein turnover

To determine protein half-life, translation was blocked by addition of cycloheximide (100 μg/ml) and cells were harvested at various times by centrifugation (800 g for 10 min at 4˚C). Cells were washed with ice-cold PBS, then resuspended in 1x SDS sample buffer (Thermo) and incubated at 70˚C for 10 min. Samples were subjected to standard SDS-PAGE electrophoresis.

Western blotting

Proteins were separated by electrophoresis on a 4-12% precast acrylamide Bis-Tris gel (Thermo) and transferred to PVDF membranes using the iBlot2 system (23 V, 6 min; Thermo). Non-specific binding was blocked using 5% (w/v) bovine serum albumin (BSA; Sigma) in Tris-buffered saline (pH 7.4) with 0.2% (v/v) Tween-20 (TBST). Membranes were incubated with primary antibodies diluted in TBST supplemented with 1% BSA overnight at 4˚C. Antibodies were used at the following dilutions: rat anti-HA epitope IgG_1 (clone 3F10; Sigma) at 1:5,000, rabbit anti-ISG75 (in house) at 1: 10,000, anti-mouse b-tubulin (clone KMX-1; Millipore) at 1: 10,000. Following five washes with TBST of 10 min each, membranes were incubated with secondary antibodies diluted in TBST supplemented with 1% BSA. Dilutions of

horseradish peroxidase (HRP)-coupled secondary antibodies (Sigma) were anti-rat-HRP at 1: 10,000, anti-rabbit-HRP at 1: 10,000, anti-mouse-HRP at 1: 10,000. Detection was carried out by incubating membranes with ECL Prime Western Blotting System (Sigma) and GE healthcare Amersham Hyperfilm ECL (GE). Densitometry quantification was conducted using ImageJ software (NIH). For quantification using the Li-COR system (Li-Cor Bioscience, Lincoln NE), the following antibodies were diluted in Odyssey blocking buffer (Li-COR): goat anti-rabbit IgG: IR Dye680RD and goat anti-mouse or anti-rat IgG: IRDye800CW (Li-COR). All washes were with PBS supplemented with 0.5% Tween20. Quantitative Fluorescence signals were quantified on an Odyssey CLx Imager and processed using Li-COR software (Li-COR).

Blue native PAGE (BN-PAGE)

BN-PAGE was performed using the NativePAGE Bis-Tris gel system (Thermo). Briefly, cells were washed three times with 1X PBS supplemented with protease inhibitor cocktail without EDTA (Roche) and solubilized in Native PAGE sample buffer supplemented with 10% glycerol, 1% n-dodecyl-b-d-maltoside, 1x protease inhibitor cocktail without EDTA (Roche), 100 μg/ml micrococcal nuclease (NEB), and 1x micrococcal nuclease buffer (NEB). Samples were incubated in solubilization buffer on ice for 30 min and centrifuged (13,000 g at 4 ˚C, 30 min). The resulting supernatants were fractionated on precast 4-16% BN gradient gels (Thermo).

Affinity isolation

Ubiquitylated proteins were isolated using the UbiQapture-Q kit (Enzo Life Sciences, Farmingdale, New York, USA) according to the manufacturer's instructions. Ubiquitylated proteins were isolated from a total of 1×10^7 cells lysed with TEN buffer (150 mM NaCl, 50 mM Tris-HCl, pH 7.4, 5 mM EDTA, 1% Triton X-100), supplemented with 100 mM N-ethylmaleimide (NEM) to inhibit deubiquitinase activity [36]. A total of 40 μl of UbiQapture-Q^{TM} matrix was pre-equilibrated in TEN buffer and incubated with cell lysates (200 μl) by rotating at 4˚C overnight. After washing five times, captured proteins were eluted with 2x SDS-PAGE sample buffer containing 10mM DTT. Samples were resolved in 4-12% acrylamide gels, transferred onto PVDF membranes and analyzed by Western blotting using anti-HA antibody in blocking buffer (TBST supplemented with 1% BSA).

Molecular modelling

A homology model of TbAQP2 tetramer (residues 68-312) was built using Modeller (version 9.20) [37,38] using as template the crystal structure of the *Homo sapiens* AQP10 (PDB code 6f7H) [39]. The N-terminus (residues 1-59) could not be modelled due to predicted flexibility and low sequence similarity. *T. brucei* AQP2 has 33% identity compared to *Homo sapiens* AQP10. Multiple sequence alignments were performed using T-Coffee [40] and ClustalW [41]. The geometries of the homology model were refined using Maestro and verified using PROCHECK [42] The resulting Ramachandran plots indicated a good model quality with 93% of the residues in most favoured regions. A second model displaying K147R and K234R mutations in each monomer was generated following the same protocol. Both models were refined using all-atom molecular dynamics (MD) simulations with Desmond [43]. Each system was embedded as a tetramer in a periodic POPC lipid bilayer generated with "System Builder" in Maestro and solvated in aqueous 150mM KCl. The OPLS3e force field was used to further improve the resulting molecular model [44]. The cut-off distance for non-bonded interactions was 9 Å. The SHAKE algorithm was applied to all bonds involving hydrogens, and an integration step of 2.0 fs was used throughout [45]. The systems were simulated with no restraints at constant temperature (300K) and pressure (1atm) for 100ns. Protein structures and MD trajectories were visually inspected and analysed using the molecular visualization programs PyMOL, VMD [45] and Maestro [43].

Results

TbAQP2 forms stable tetrameric complexes in the bloodstream form of T. brucei

TbAQP2 (Tb927.10.14170) is critical for water and glycerol transport activity as well as sensitivity to diamidines and melaminophenyl arsenicals in African trypanosomes [13,23,33]. A recent study suggested that pentamidine may be a nanomolar ligand, rather than a transport substrate of TbAQP2 [22] and that endocytosis of TbAQP2 might be important for pentamidine transport. However, the intracellular and surface trafficking pathways of AQPs in trypanosomes have not been elucidated. Central to endocytosis and protein sorting of many surface membrane proteins is ubiquitylation [46], and ubiquitylation of the type I surface-localised invariant surface glycoproteins 65 and 75 (ISG65 and ISG75) is essential for internalization and degradation in the lysosome [33,47,48].

To determine whether ubiquitylation is involved in trafficking and turnover of polytopic surface proteins in trypanosomes we addressed whether TbAQP2 is ubiquitylated *in vivo*. We generated *T. brucei* cell lines expressing TbAQP2 tagged at the N- ($^{3\times HA}$AQP2) or C-terminus (AQP2$^{3\times HA}$) (**Fig 1A and B**) using an *aqp*-null cell line [19] as chassis to prevent heterologous interaction with endogenous AQPs. The hemagglutinin (HA) tag was selected as it lacks lysine residues (as opposed to more bulky tags such as GFP) and therefore is incapable of becoming ubiquitylated and interfering with data interpretation. Both constructs co-localized with ISG75 at the posterior end of the cell, consistent with the location of native AQP2 at the flagellar pocket (**Fig 2A**). $^{3\times HA}$AQP2 is predominantly detected as two forms by immunoblotting after SDS-PAGE: a ~38 kDa form, consistent with the monomeric form, and a >120 kDa form, likely a homotetramer (**Fig 2B, lower panel**), as previously reported for other AQPs [16,49–51]. In sharp contrast, AQP2$^{3\times HA}$ was found as two main species of ~35 kDa and ~38 kDa, with no tetrameric form detected (**Fig 2B, lower panel**). However, under native conditions, both constructs are organized as high molecular weight complexes of ~480 kDa, consistent with a 4x4 conformation under native conditions (**Fig 2B, upper panel**).

Thus, whereas $^{3\times HA}$AQP2 is readily detectable as a stable tetramer, even under harsh conditions, AQP2$^{3\times HA}$ is comparatively less stable in its tetrameric form (**Fig 2B**), likely indicating interference by the C-terminal HA tag to oligomerization and/or tetramer stability. To determine the glycerol transport capacity of these proteins, we inhibited the activity of the trypanosome alternative oxidase (TAO) with salicylhydroxamic acid (SHAM) [21]. Inhibition of TAO leads to increased intracellular glycerol, building up to toxic levels that can only be prevented by export *via* a glycerol transporter such as AQP. Therefore, the absence of functional AQPs renders cells highly susceptible to SHAM. Consistent with stability of the AQP2^{3xHA} oligomeric form, expression of the $^{3\times HA}$AQP2 construct in the *aqp-null* background restored sensitivity to pentamidine and glycerol transport comparable to wild type cells, whereas AQP2$^{3\times HA}$ only partly rescued these phenotypes (**Fig 2C and S1 Fig**). Both $^{3\times HA}$AQP2 and AQP2$^{3\times HA}$ have long half-lives (>4h) (**Fig 2D**) indicating that impaired transport activity of AQP2^{3xHA} is unlikely due to altered turnover or structure. Therefore, although introduction of HA epitopes to either terminus does not alter localization, only the N-terminal tagged form assembles stable oligomeric structures and fully functional TbAQP2. Therefore, we selected to focus on ^{3xHA}AQP2.

TbAQP2 is ubiquitylated and degraded by the lysosome

Next, we sought evidence that TbAQP2 is ubiquitylated. Cycles of protein ubiquitylation and deubiquitylation are important for controlling the cell surface composition of trypanosomes [25,33,52]. Both proteasome-dependent and lysosome-mediated protein degradation are generally initiated by covalent attachment of one or more ubiquitin moieties to a substrate protein [53], and we rationalized that inhibiting these degradative systems would increase the overall abundance of ubiquitylated intermediates.

We observed high molecular weight adducts when cells expressing $^{3\times HA}$AQP2 were treated with either ammonium chloride (lysosomal activity inhibitor) or MG132 (proteasome inhibitor) (**Fig 3A**), likely representing ubiquitylated intermediates *en route* to degradation. Subsequent western blotting identified a predominant band of ~55 kDa reactive to anti-ubiquitin antibody upon immunoprecipitation with anti-HA magnetic beads, consistent with the addition of ubiquitin to TbAQP2 (~38 kDa for unmodified protein (**Fig 3B**). To corroborate these results, we performed an affinity isolation using a commercial ubiquitin binding domain (UBD) resin followed by western blotting with anti-HA antibody. This revealed unmodified monomer together with high molecular weight adducts, likely representing TbAQP2 with various numbers of ubiquitin conjugates; the latter clearly represents a small fraction of total AQP2 expressed in these cells (**Fig 3C**). Interestingly, we noted a band of around ~40 kDa, likely corresponding to monoubiquitylated TbAQP2 (**Fig 3C**). Collectively, these results indicate that TbAQP2 is modified by ubiquitin in the bloodstream form of *T. brucei*.

Next, we sought to investigate the mechanisms by which TbAQP2 is degraded. Imaging suggested that TbAQP2 is predominantly located at the flagellar pocket together with ISG75, but a proportion is also in close proximity to early endosomes (positive for Rab5A and Rab5B) but less so for recycling endosomes (Rab11) (**Fig 4A**) suggesting transit of TbAQP2 through early endosomes. Moreover, TbAQP2 displayed strong overlap with p67, a lysosomal marker, suggesting that TbAQP2 is delivered to the lysosome *via* endocytosis (**Fig 4A**). Similar observations were made with cells expressing AQP2$^{3\times HA}$ (**S2 fig**), once more indicating that the C-terminal tag does not impair trafficking but rather hinders oligomerisation. Further, pulse-chase analysis showed that ISG75 has a half-life of ~3.6 h, consistent with earlier studies [33,47,48]**,** whereas TbAQP2 displays bimodal behaviour with approximately half

rapidly turned over in <1 h, with the remaining fraction is more stable, with a half-life of ~6 h (**Fig 4B**), which together with partial juxtaposition with Rab11, suggests possible recycling. To determine whether TbAQP2 is degraded in the lysosome or the proteasome we treated cells with bafilomycin A1 (BafA1; inhibitor of the lysosomal v-ATPase) or MG132 (canonical proteasome inhibitor with broad-range inhibitory capacity against serine proteases and calpain-like proteases [54]). In untreated cells, TbAQP2 was reduced by ~50% after 1 h as expected, but in cells treated with BafA1 or MG132, less that 20% of the protein was degraded (**Fig 4C**). It is important to note that MG132 can also impair degradation of proteins delivered to the lysosome as it acts as a broad range inhibitor for lysosome-specific proteases [54]. Overall, these data indicate that TbAQP2 is ubiquitylated and delivered to the lysosome for degradation, *albeit* with a pool of longer-lived protein that may constitute a recycling population.

Intracellular N-terminal lysine residues are essential for oligomerisation and channel function of TbAQP2

Predictions of TbAQP2 topology [55] suggested cytosolic localisations for both N- and C-termini, as is known for the mammalian orthologues (**S3 Fig,** [15,56]). AQP2 has five lysine residues that are exposed to the cytosol, at positions 19, 45, 54, 147, and 234 (**Fig 1B**). To better understand the potential ubiquitylation sites in TbAQP2, we used UbPred (http://www.ubpred.org) [57] to predict lysine residues as candidate ubiquitin acceptors. UbPred suggested that lysine residues in position 19, 45, and 54 are potential ubiquitylation sites in TbAQP2, with prediction scores of 0.65, 0.73, and 0.88, respectively. All three residues are located within the N-terminal cytoplasmic region of AQP2 (**Fig 1B**).

To dissect the contribution of these residues to TbAQP2 localisation and function, we generated a cell line expressing N-terminally tagged AQP2 in which all three of these lysine residues were simultaneously mutated ($AQP2^{3K>R}$). Unexpectedly, while the wild-type protein located in the posterior end of the cell, $AQP2^{3K>R}$ was mislocalized (**Fig 5A**) and failed to restore pentamidine sensitivity and glycerol transport (**Fig 5B**). Furthermore, whereas $AQP2^{WT}$ co-localises with ISG75 at the posterior end of the cells, $AQP2^{3K>R}$ was retained in the endoplasmic reticulum (ER), as suggested by co-localisation with the ER marker TbBiP (**Fig 5C**). Blue native-PAGE indicated that whereas $AQP2^{WT}$ forms two high molecular weight complexes (~480 kDa and ~120 kDa), $AQP2^{3K>R}$ did not oligomerise (**Fig 5D and S4 Fig**).

Moreover, AQP2$^{3K>R}$ is highly unstable and turned over faster than AQP2^{WT} and in an MG-132 selective manner (**Fig 5E**). We conclude that K19, K45 and K54 are essential for TbAQP2 folding and hence anterograde trafficking and that their replacement by arginine triggers entry into an ER-associated degradative (ERAD) pathway [58–60].

Site-directed mutation of cytoplasmic lysine residues of TbAQP2 leads to protein instability

To determine whether the effects observed for AQP2$^{3K>R}$ could be attributed to a single lysine residue we generated a construct in which all cytoplasmic lysine residues were mutagenized to arginine (AQP2$^{5K>R}$) (**Fig 1B**). Using this construct as template, we reverted each lysine individually using site-directed mutagenesis, generating cell lines expressing N-terminally tagged mutant TbAQP2 with only one lysine residue reinstated (AQP2^{R19K}, AQP2^{R45K}, and AQP2^{R54K}). None of these mutants formed oligomers (**S4A Fig.**) and were retained in the ER, as demonstrated by co-localisation with TbBiP (**Fig 6A**). Moreover, AQP2$^{5K>R}$, AQP2^{R19K}, AQP2^{R45K}, and AQP2^{R54K} turn over faster than AQP2^{WT} and are stabilised by MG-132 (**Fig 6B and Table 1**), consistent with the absence of detection by BN-PAGE analysis and the lack of sensitivity to pentamidine and glycerol transport observed in these mutants (**Fig 6C**). Similar results were obtained with AQP2^{R234K} (**S4F Fig**). K234 is located within the TM4-TMD5 loop, an important feature of TbAPQ2 as this loop is predicted to interact with the TM4-TM5 loop of the neighbouring subunit to create a large oligomerization interface (**S4G Fig, left panel**).

Molecular dynamics (MD) simulations of TbAQ2^{WT} and TbAQ2$^{K147R/K234R}$ suggest that the K234R mutation will likely have a notable effect on the position of the TM4-TM5 loop, hampering oligomerization (**S4G Fig**). It is important to note that we failed to successfully express AQP2^{R147K} despite multiple independent transfections. Residue 147 is located between TMD4 and TMD5, potentially indicating that mutation of this residue leads to a far more unstable protein than the other constructs, and in good agreement with the MD simulations. In TbAQP2^{WT}, K147 is predicted to interact with Y151 and N70 on TMD1 and maintain the TMD3-TMD1 interface (**S4G Fig, right panel).** On the other hand, simulations of TbAQP2$^{K147R/K234R}$ showed a significant conformational change of TMD1 and TMD3 as a result of establishment of a salt bridge between R234 and D73 on TMD1. This conformational change on TMD1 would impact both the conformation of the N-terminal tail and the dimerization interface with TMD6 from the neighbouring subunit, providing a rationale for the instability observed in this

mutant. Consistent with a lack of oligomerization and rapid turnover all of these constructs failed to restore pentamidine sensitivity or glycerol transport (**Fig 6C and Table 1**).

Chimerization of TbAQP2 impairs stability, localization and function

T. brucei possesses three AQP paralogues [21,23]. Of these, TbAQP2 and TbAQP3 are tandem open reading frames located on chromosome 10 and share >70% protein identity [13]. Chimerisation of the loci encoding TbAQP2 and TbAQP3 causes resistance to pentamidine and melarsoprol [27,29,32,56]. Interestingly, although in some cases the selectivity pore is mutated, many chimeric AQP2/3 alleles do not have altered amino acids in the selectivity pore, but rather replacement of TMD regions with sequences from TbAQP3 (**Fig 1C**), [29–32]. Moreover, the AQP2/3 chimeras characterised so far display a subcellular localisation resembling TbAQP3 at the plasma membrane, in contrast with an expected flagellar pocket localisation for TbAQP2 (**Fig 2A**) [27]. However, it is unclear if TbAQP2 chimerisation impacts additional features beyond subcellular localisation.

We generated cell lines expressing tetracycline-regulated N-terminal tagged TbAQP1, TbAQP2, TbAQP3 and the chimeric AQP2/3 40AT (40AT) (**Fig 1C**), isolated from relapse patients from the Democratic Republic of Congo [29]. One of the main structural features of this chimera is replacement of the sixth *trans*-membrane and C-terminus of TbAQP2 with the corresponding sequence of TbAQP3 (**Fig 1C**) [29]. Additionally, to simulate other chimeric AQP2/3 proteins identified in laboratory strains and field isolates, we generated AQP2 mutants where TMD4 ($AQP2^{TMD4}$) and TMD5 ($AQP2^{TMD5}$) are individually replaced by the corresponding TMDs from TbAQP3 (**Fig 1C**). Apart from the $AQP2^{TMD5}$ construct, none of these constructs alter the amino acid composition of the selectivity filter of TbAQP2 (**S5 and S6 Fig**). Whereas we readily expressed $AQP2^{TMD4}$, we failed to obtain positive clones for $AQP2^{TMD5}$, despite multiple attempts. We observed that TbAQP2 colocalised with ISG75, as expected, as well as TbAQP1 which seems to localise in close proximity to ISG75, whereas TbAQP3 localises mainly to the cell surface as previously reported [13,21] (**Fig 7A, left-hand panel**). Conversely, $AQP2^{TMD4}$ and the clinical chimera 40AT displayed a distinct localisation in proximity with TbBiP (**Fig 8A**). Western blotting showed that under reducing conditions, all these constructs are readily detected as monomers of ~35-38 kDa (**Fig 7A, right-hand panel**). Under native conditions, both TbAQP1 and TbAQP2 can be readily detected as *n*-dodecyl b-D-maltoside (DDM)-soluble forms of

~480 kDa species, consistent with the proposed 4x4 organization, whereas we failed to observe such complexes for TbAQP3, 40AT, and AQP2^{TMD4} (**Fig 7B**). TbAQP3, AQP2^{TMD4} and 40AT are turned over more rapidly (<1 h) than TbAQP1 and TbAQP2 (**Fig 7D and Table 2**), explaining the lack of glycerol transport in cells expressing these constructs (**Fig 7C**).

The localisation of TbAQP3 and the chimeric AQP2-3 proteins is reminiscent of the subcellular localization observed in the lysine-to-arginine TbAQP2 mutants. Based on these observations we hypothesised that these constructs are likely to be retained in the ER, at least to a level comparable to that of the lysine-to-arginine TbAQP2 mutants. We observed that whereas TbAQP1 and TbAQP2 show poor co-localisation with TbBiP, the signal of TbAQP3 and 40AT partly co-localised with this ER marker, indicating some degree of retention within this organelle (**Fig 8A**). Moreover, TbAQP3 and 40AT turnover was faster than TbAQP1 and TbAQP2 and was significantly impaired in the presence MG132 but not bafilomycin A1(**Fig 8B**), indicating that these constructs are retained and degraded in the ER and not in the lysosome, as observed for TbAQP2.

Discussion

Aquaporins are present throughout prokaryotes and eukaryotes [15–17], and have conserved topology and quaternary structure. AQPs form homotetrameric complexes to transport water and low molecular weight solutes [15–17]. Independent expansions of AQP paralogues have served to diversify function and in mammals and *Leishmania major* both ubiquitylation and phosphorylation are important in modulating turnover and hence activity [61–66]. Significantly, the three trypanosome AQP paralogs derive from a single ancestral gene shared with *Leishmania spp.*, and thus relative functions of paralogs are likely differentially distributed between major lineages. Despite clear clinical importance, little is known concerning AQP trafficking and higher order assembly in trypanosomes and specifically the impact of mutations on these properties. We found that TbAQP2 assembles into high molecular weight complexes that potentially resemble the quasi-arrays described for HsAQP4 [67–71]. Oligomerization correlates with bidirectional glycerol flow but also pentamidine sensitivity as C-terminal tagged forms form oligomers with low efficiency and have

poor transport activity. Furthermore, TbAQP2 is ubiquitylated and targeted to the lysosome, similar to mammalian AQPs [62].

Pentamidine is thought to be taken up *via* translocation by and/or endocytosis of TbAQP2 [22,56]. If endocytosis were the sole route and assuming that lysosomal delivery is required, a faster turnover rate than ~1 h would be necessary to achieve the intracellular pentamidine levels observed, i.e. ~16 pmol pentamidine/10^7 cells per hour [72]. Neither pentamidine nor melarsoprol sensitivity requires an obvious lysosomal transporter, suggesting that channel-mediated transport is required, regardless of any endocytic contribution. However, the intrinsic instability of several tagged TbAQP2 mutants precluded detailed dissection of uptake pathways as all of the lysine to arginine mutations led to ER retention [59,60]. As specific mutation of selectivity pore residues does not alter localisation to the flagellar pocket, residues elsewhere are more important for efficient folding.

All *T. brucei* AQP paralogs are predicted as topologically similar, but nevertheless possess distinct properties and subcellular localisations [13,18–23,73]. TbAQP2 is essential for pentamidine and melarsoprol uptake [13], while TbAQP3 is associated with susceptibility to antimonial compounds including sodium stibogluconate [71], indicating transport specificity. Trypanosomes from patients following melarsoprol treatment failure possess a mutated AQP2/3 locus [20,28,29,56,74], with single nucleotide polymorphisms, AQP2 deletions and several fusions replacing TbAQP2 TMD4, 5 or 6 with TbAQP3 sequences, in most cases without impacting the NPA/NPA and WGYR selectivity pore motifs [29,31,32]. Several chimeras have aberrant subcellular localisations [20,28,29,56,74], indicating that the selectivity filters is comparatively unimportant for targeting. Consistent with this is that both TbAQP1 and TbAQP2 assemble into higher order complexes but TbAQP3 apparently does so less efficiently. Similarly, TbAQP1 and TbAPQ2 have a long half-life ($t_{1/2}$ >4 h) and restricted subcellular localisation around the flagellar pocket, whereas TbAQP3 is comparatively short-lived ($t_{1/2}$ ~1 h) and localises mainly to the cell body surface, suggesting a connection between oligomerisation, stability, subcellular localisation and transport activity [67,69–71]. Furthermore, replacement of TMD4 or 6 in TbAQP2 by TbAQP3 sequences (we were unable to generate TMD5 chimeras), as observed in clinically relevant chimeric AQP2-3, led to impaired oligomerisation, ER-retention and decreased stability, strengthening the correlation between oligomerisation, localisation and function.

In summary, we propose that pentamidine uptake depends upon the structural organisation of TbAQP2 and that channel activity is essential. Furthermore, TbAQP2 is highly sensitive to mutation and/or chimerisation, which results in failure to correctly fold and ER-retention. This mechanism most likely accounts for many instances of clinically observed pentamidine and melarsoprol resistance.

Acknowledgements

This work was supported by grants from the Wellcome Trust (204697/Z/16/Z to MCF and 1000320/Z/12/Z to DH) and the Medical Research Council (MR/P009018/1 to MCF). We are grateful to Dave Ng for assistance with sample preparation for imaging and to Martin Zoltner and Ricardo Canavate del Pino for helpful discussions during the preparation of this manuscript. We are also grateful to Pascal Mäser (Swiss Tropical and Public Health Institute) for providing the 40AT chimera.

References

1. Capewell P, Atkins K, Weir W, Jamonneau V, Camara M, Clucas C, et al. Resolving the apparent transmission paradox of African sleeping sickness. PLoS Biol. 2019;17:e3000105.
2. Brun R, Blum J, Chappuis F, Burri C. Human African trypanosomiasis. Lancet. 2010;375:9–15.
3. Mehlitz D, Molyneux DH. The elimination of Trypanosoma brucei gambiense? Challenges of reservoir hosts and transmission cycles : Expect the unexpected. Parasite Epidemiol Control. 2020;6:e00113.
4. Selby R, Wamboga C, Erphas O, Mugenyi A, Jamonneau V, Waiswa C, et al. Gambian human African trypanosomiasis in North West Uganda . Are we on course for the 2020 target ? PLoS Negl Trop Dis. 2019;13:e0007550.
5. Maclean L, Reiber H, Kennedy PGE, Sternberg JM. Stage Progression and Neurological Symptoms in Trypanosoma brucei rhodesiense Sleeping Sickness : Role of the CNS Inflammatory Response. PLoS Negl Trop Dis. 2012;6:e1857.
6. Baker N, Koning HP De, Mäser P, Horn D. Drug resistance in African trypanosomiasis : the melarsoprol and pentamidine story. Trends Parasitol. 2013;29.
7. Field MC, Horn D, Fairlamb AH, Ferguson MAJ, Gray DW, Read KD, et al. Anti-trypanosomatid drug discovery: An ongoing challenge and a continuing need. Nat

516 Rev Microbiol. 2017;15:217–31.
517 8. Mesu VKBK, Kalonji WM, Bardonneau C, Mordt OV, Blesson S, Simon F, et al.
518 Oral fexinidazole for late-stage African Trypanosoma brucei gambiense
519 trypanosomiasis: a pivotal multicentre, randomised, non-inferiority trial. Lancet.
520 2017;391:144–54.
521 9. Wall RJ, Rico E, Lukac I, Zuccotto F, Elg S, Gilbert IH, et al. Clinical and
522 veterinary trypanocidal benzoxaboroles target CPSF3. Proc Natl Acad Sci U S A.
523 2018;115:9616–21.
524 10. Pandey A, Galvani A. Strategies for Trypanosoma brucei gambiense elimination.
525 Lancet Glob Heal. 2017;5:10–1.
526 11. Acup C, Bardosh KL, Picozzi K, Waiswa C, Welburn SC. Factors influencing
527 passive surveillance for T. b. rhodesiense human african trypanosomiasis in
528 Uganda. Acta Trop. 2017;165:230–9.
529 12. Alsford S, Eckert S, Baker N, Glover L, Sanchez-Flores A, Leung KF, et al. High-
530 throughput decoding of antitrypanosomal drug efficacy and resistance. Nature.
531 2012;482:232–6.
532 13. Baker N, Glover L, Munday JC, Aguinaga Andres D, Barrett MP, de Koning HP,
533 et al. Aquaglyceroporin 2 controls susceptibility to melarsoprol and pentamidine in
534 African trypanosomes. Proc Natl Acad Sci. 2012;109:10996–1001.
535 14. De Koning HP. Uptake of pentamidine in Trypanosoma brucei brucei is mediated
536 by three distinct transporters: implications for cross-resistance with arsenicals. Mol
537 Pharmacol. 2001;59:586–92.
538 15. Verkman AS. Aquaporins at a glance. J Cell Sci. 2011;124:2107–12.
539 16. Verkman AS, Anderson MO, Papadopoulos MC. Aquaporins: important but
540 elusive drug targets. Nat Rev Drug Discov. 2014;13:259–77.
541 17. Hub JS, de Groot BL. Mechanism of selectivity in aquaporins and
542 aquaglyceroporins. Proc Natl Acad Sci. 2008;105:1198–203.
543 18. Berriman M, Ghedin E, Hertz-Fowler C, Blandin G, Renauld H, Bartholomeu DC,
544 Lennard NJ, Caler E, Hamlin NE, Haas B, Böhme U, Hannick L, Aslett MA, Shallom
545 J, Marcello L, Hou L, Wickstead B, Alsmark UC, Arrowsmith C, Atkin RJ, Barron AJ,
546 Bringaud F, Brooks E-SN. The genome of the African trypanosome Trypanosoma
547 brucei. Science (80-). 2005;309:416–22.
548 19. Beitz E. Aquaporins from pathogenic protozoan parasites: structure, function and
549 potential for chemotherapy. Biol Cell. 2005;97:373–83.

550 20. Schmidt RS, Macêdo JP, Steinmann ME, Salgado AG, Bütikofer P, Sigel E, et al.
551 Transporters of Trypanosoma brucei—phylogeny, physiology, pharmacology. FEBS
552 J. 2018;285:1012–23.
553 21. Jeacock L, Baker N, Wiedemar N, Maser P, Horn D, Maser P, et al.
554 Aquaglyceroporin-null trypanosomes display glycerol transport defects and
555 respiratory-inhibitor sensitivity. PLoS Pathog. 2017;13:1–16.
556 22. Song J, Baker N, Rothert M, Henke B, Jeacock L, Horn D, et al. Pentamidine Is
557 Not a Permeant but a Nanomolar Inhibitor of the Trypanosoma brucei
558 Aquaglyceroporin-2. PLoS Pathog. 2016;12:1–14.
559 23. Bassarak B, Uzcátegui NL, Schönfeld C, Duszenko M. Functional
560 Characterization of Three Aquaglyceroporins from Trypanosoma brucei in
561 Osmoregulation and Glycerol Transport. Cell Physiol Biochem. 2011;27:411–20.
562 24. Uzcategui NL, Szallies A, Pavlovic-Djuranovic S, Palmada M, Figarella K,
563 Boehmer C, et al. Cloning, heterologous expression, and characterization of three
564 aquaglyceroporins from Trypanosoma brucei. J Biol Chem. 2004;279:42669–76.
565 25. Quintana JF, Del Pino RC, Yamada K, Zhang N, Field MC. Adaptation and
566 therapeutic exploitation of the plasma membrane of African trypanosomes. Genes.
567 2018;9.
568 26. Sui H, Han B, Lee J, Walian P, Jap B. Structural basis of water-specific transport
569 through the AQP1 water channel. Nature. 2001;414:872–8.
570 27. Munday JC, Eze AA, Baker N, Glover L, Clucas C, Andrés DA, et al.
571 Trypanosoma brucei aquaglyceroporin 2 is a high-affinity transporter for pentamidine
572 and melaminophenyl arsenic drugs and the main genetic determinant of resistance
573 to these drugs. J Antimicrob Chemother. 2014;69:651–63.
574 28. Graf FE, Baker N, Munday JC, de Koning HP, Horn D, Mäser P. Chimerization at
575 the AQP2-AQP3 locus is the genetic basis of melarsoprol-pentamidine cross-
576 resistance in clinical Trypanosoma brucei gambiense isolates. Int J Parasitol Drugs
577 Drug Resist. 2015;5:65–8.
578 29. Graf FE, Ludin P, Wenzler T, Kaiser M, Brun R, Pyana PP, et al. Aquaporin 2
579 Mutations in Trypanosoma brucei gambiense Field Isolates Correlate with
580 Decreased Susceptibility to Pentamidine and Melarsoprol. PLoS Negl Trop Dis.
581 2013;7.
582 30. Unciti-Broceta JD, Arias JL, Maceira J, Soriano M, Ortiz-González M,
583 Hernández-Quero J, et al. Specific Cell Targeting Therapy Bypasses Drug

584 Resistance Mechanisms in African Trypanosomiasis. PLoS Pathog. 2015;11:1–20.
585 31. Pyana PP, Lukusa IN, Ngoyi DM, van Reet N, Kaiser M, Shamamba SK Bin, et
586 al. Isolation of Trypanosoma brucei gambiense from cured and relapsed sleeping
587 sickness patients and adaptation to laboratory mice. PLoS Negl Trop Dis. 2011;5:1–
588 6.
589 32. Graf FE, Baker N, Munday JC, Koning HP De, Horn D, Mäser P. Chimerization
590 at the AQP2 – AQP3 locus is the genetic basis of melarsoprol – pentamidine cross-
591 resistance in clinical Trypanosoma brucei gambiense isolates. Int J Parasitol Drugs
592 Drug Resist. 2015;5:65–8.
593 33. Zoltner M, Leung KF, Alsford S, Horn D, Field MC. Modulation of the Surface
594 Proteome through Multiple Ubiquitylation Pathways in African Trypanosomes. PLoS
595 Pathog. 2015;11:1–26.
596 34. Raz B, Iten M, Grether-Buhler Y, Kaminsky R, Brun R. The Alamar Blue® assay
597 to determine drug sensitivity of African trypanosomes (T.b. rhodesiense and T.b.
598 gambiense) in vitro. Acta Trop. 1997;68:139–47.
599 35. Currier RB, Cooper A, Burrell-Saward H, MacLeod A, Alsford S. Decoding the
600 network of Trypanosoma brucei proteins that determines sensitivity to
601 apolipoprotein-L1. PLoS Pathog. 2018;14:1–26.
602 36. Emmerich CH, Cohen P. Optimising methods for the preservation , capture and
603 identi fi cation of ubiquitin chains and ubiquitylated proteins by immunoblotting.
604 Biochem Biophys Res Commun. 2016;466:1–14.
605 37. Sali A, Blundell T. Comparative protein modelling by satisfaction of spatial
606 restraints. J Mol Biol. 1993;234:779–815.
607 38. Webb B, Sali A. Comparative Protein Structure Modeling Using MODELLER.
608 Curr Protoc Bioinforma. 2016;54.
609 39. Gotfryd K, Mosca A, Missel J, Truelsen S, Wang K, Spulber M, et al. Human
610 adipose glycerol flux is regulated by a pH gate in AQP10. Nat Commun.
611 2018;9:4749.
612 40. Notredame C, Higgins D, Heringa J. T-Coffee: A novel method for fast and
613 accurate multiple sequence alignment. J Mol Biol. 2000;302:205–17.
614 41. Thompson J, Higgins D, Gibson T. CLUSTAL W: improving the sensitivity of
615 progressive multiple sequence alignment through sequence weighting, position-
616 specific gap penalties and weight matrix choice. Nucleic Acids Res. 1994;22:4673–
617 80.

618 42. Laskowski R, MacArthur M, Moss D, Thornton J. PROCHECK: a program to
619 check the stereochemical quality of protein structures. J Appl Cyrstallography.
620 1993;26:283–91.
621 43. Bowers KJ, Chow E, Xu H, Dror RO, Eastwood MP, Gregersen BA, et al.
622 Scalable Algorithms for Molecular Dynamics Simulations on Commodity Clusters.
623 Proc ACM /. 2006;11–7.
624 44. Harder E, Damm W, Maple J, Wu C, Reboul M, Xiang JY, et al. OPLS3: A Force
625 Field Providing Broad Coverage of Drug-like Small Molecules and Proteins. J Chem
626 Theory Comput. 2016;12:281–96.
627 45. Ryckaert J-P, Ciccotti G, Berendsen HJC. Numerical integration of the cartesian
628 equations of motion of a system with constraints: molecular dynamics of n-alkanes. J
629 Comput Phys. 1977;23:327–41.
630 46. Piper RC, Dikic I, Lukacs GL. Ubiquitin-Dependent Sorting in Endocytosis. Cold
631 Spring Harb Perspect Biol. 2014;6:a016808.
632 47. Chung W-LL, Leung KF, Carrington M, Field MC. Ubiquitylation is required for
633 degradation of transmembrane surface proteins in Trypanosomes. Traffic.
634 2008;9:1681–97.
635 48. Leung KF, Riley FS, Carrington M, Field MC. Ubiquitylation and developmental
636 regulation of invariant surface protein expression in trypanosomes. Eukaryot Cell.
637 2011;10:916–31.
638 49. Klein N, Neumann J, O'Neil JD, Schneider D. Folding and stability of the
639 aquaglyceroporin GlpF: Implications for human aquaglyceroporin diseases. Biochim
640 Biophys Acta - Biomembr. 2015;1848:622–33.
641 50. Cymer F, Schneider D. A single glutamate residue controls the oligomerization,
642 function, and stability of the aquaglyceroporin GlpF. Biochemistry. 2010;49:279–86.
643 51. Schmidt V, Sturgis JN. Making Monomeric Aquaporin Z by Disrupting the
644 Hydrophobic Tetramer Interface. ACS Omega. 2017;2:3017–27.
645 52. Zoltner M, Horn D, de Koning HP, Field MC. Exploiting the Achilles' heel of
646 membrane trafficking in trypanosomes. Curr Opin Microbiol. 2016;34:97–103.
647 53. J.Clague M, Urbé S. Ubiquitin: Same Molecule, Different Degradation Pathways.
648 Cell. 2010;143:682–5.
649 54. Tsubuki S, Saito Y, Tomioka M, Ito H, Kawashima S. Differential inhibition of
650 calpain and proteasome activities by peptidyl aldehydes of di-leucine and tri-leucine.
651 J Biochem. 1996;119:572–6.

652 55. Krogh A, Larsson È, Heijne G Von, Sonnhammer ELL. Predicting
653 Transmembrane Protein Topology with a Hidden Markov Model : Application to
654 Complete Genomes. J Mol Biol. 2001;305:567–80.
655 56. Munday JC, Settimo L, de Koning HP. Transport proteins determine drug
656 sensitivity and resistance in a protozoan parasite, Trypanosoma brucei. Front
657 Pharmacol. 2015;6:1–10.
658 57. Radivojac, P., Vacic, V., Haynes, C., Cocklin, R. R., Mohan, A., Heyen, J. W.,
659 Goebl, M. G., and Iakoucheva LM. Identification, Analysis and Prediction of Protein
660 Ubiquitination Sites. Proteins Struct Funct Bioinforma. 2010;78:365–80.
661 58. Carrington M, Field MC, Sergeenko T, Wang Y, Bo S. Chaperone Requirements
662 for Biosynthesis of the Trypanosome Variant Surface Glycoprotein. PLoS One.
663 2010;5:e8468.
664 59. Tiengwe C, Koeller CM, Bangs JD, Gilmore R. Endoplasmic reticulum –
665 associated degradation and disposal of misfolded GPI-anchored proteins in
666 Trypanosoma brucei. Mol Biol Cell. 2018;29:2397–409.
667 60. Tiengwe C, Muratore KA, Bangs JD. Surface proteins , ERAD and antigenic
668 variation in Trypanosoma brucei. Cell Microbiol. 2016;18:1673–88.
669 61. Mandal G, Sharma M, Kruse M, Sander-Juelch C, Munro LA, Wang Y, et al.
670 Modulation of Leishmania major aquaglyceroporin activity by a mitogen-activated
671 protein kinase. Mol Microbiol. 2012;85:1204–18.
672 62. Sharma M, Mandal G, Mandal S, Bhattacharjee H. Functional role of lysine 12 in
673 Leishmania major AQP1. Mol Biochem Parasitol. 2015;201:139–45.
674 63. Tamma G, Robben JH, Trimpert C, Boone M, Deen PMT. Regulation of AQP2
675 localization by S256 and S261 phosphorylation and ubiquitination. AJP Cell Physiol.
676 2011;300:C636–46.
677 64. Lu HJ, Matsuzaki T, Bouley R, Hasler U, Qin Q-H, Brown D. The phosphorylation
678 state of serine 256 is dominant over that of serine 261 in the regulation of AQP2
679 trafficking in renal epithelial cells. Am J Physiol Renal Physiol. 2008;295:F290-4.
680 65. Nejsum LN, Zelenina M, Aperia A, Frøkiaer J, Nielsen S. Bidirectional regulation
681 of AQP2 trafficking and recycling: involvement of AQP2-S256 phosphorylation. Am J
682 Physiol Renal Physiol. 2005;288:F930–8.
683 66. Kamsteeg EJ, Hendriks G, Boone M, Konings IBM, Oorschot V, van der Sluijs P,
684 et al. Short-chain ubiquitination mediates the regulated endocytosis of the aquaporin-
685 2 water channel. Proc Natl Acad Sci. 2006;103:604073103.

686 67. Kitchen P, Conner MT, Bill RM, Conner AC. Structural Determinants of
687 Oligomerization of the Aquaporin-4 Channel. J Biol Chem. 2016;291:6858–71.
688 68. Crane JM, Bennett JL, Verkman AS. Live Cell Analysis of Aquaporin-4 M1 / M23
689 Interactions and Regulated Orthogonal Array Assembly in Glial Cells. J Biol Chem.
690 2009;284:35850–60.
691 69. Jin B, Rossi A, Verkman AS. Model of Aquaporin-4 Supramolecular Assembly in
692 Orthogonal Arrays Based on Heterotetrameric Association of M1-M23 Isoforms.
693 Biophys J. 2011;100:2936–45.
694 70. Furman CS, Gorelick-feldman DA, Davidson KG V., Yasumura T, Neely JD, Agre
695 P, et al. Aquaporin-4 square array assembly : Opposing actions of M1 and M23
696 isoforms. Proc Natl Acad Sci. 2003;100:13609–14.
697 71. Silberstein C, Bouley R, Huang Y, Fang P, Pastor-soler N, Brown D, et al.
698 Membrane organization and function of M1 and M23 isoforms of aquaporin-4 in
699 epithelial cells. Am J Physiol Renal Physiol. 2004;287:501–11.
700 72. De Koning HP. Uptake of pentamidine in Trypanosoma brucei brucei is mediated
701 by three distinct transporters: Implications for cross-resistance with arsenicals. Mol
702 Pharmacol. 2001;59:586–92.
703 73. Collett CF, Kitson C, Baker N, Steele-Stallard HB, Santrot M-V, Hutchinson S, et
704 al. Chemogenomic Profiling of Antileishmanial Efficacy and Resistance in the
705 Related Kinetoplastid Parasite Trypanosoma brucei . Antimicrob Agents Chemother.
706 2019;63:1–19.
707 74. Fairlamb AH, Horn D. Melarsoprol Resistance in African Trypanosomiasis.
708 Trends Parasitol. 2018;34:481–92.
709
710
711
712
713
714
715
716
717
718

Figure legends

Figure 1. Schematic representation of constructs used in this study. A) 3D structural predictions of the AQP2 harbouring three haemagglutinin tags at either terminus. **Top panel**; lateral and cytoplasmic face view of simulated model of *T. brucei* AQP2 tetramer embedded in a POPC lipid bilayer. Lipids are shown in surface and line representations in cyan. Each monomer of AQP2 is shown in cartoon representation. **Bottom panel**; lateral and cytoplasmic face view of *T. brucei* AQP2 showing key amino acids (in spheres) from NSA (cyan), NPS (orange) and IVLL (magenta) domains. **B)** N- and C-terminal tagged TbAQP2 variants with a tandem of three hemagglutinin (3xHA) epitopes. Positions of predicted *trans*-membrane domains (TMD) are indicated with numbers above solid blocks. Similarly, lysine residues that were manipulated in this study are highlighted. **C)** Wild type TbAQP1 (blue), TbAQP2 (grey), TbAQP3 (green), and chimeras used (40AT, AQP2^{TMD4}, and AQP2^{TMD5}). TMDs for AQP1, 2 and 3 are shown as blocks and in blue, grey and green, respectively.

Figure 2. Characterisation of tagged TbAQP2. **A)** Fluorescence microscopy of *T. brucei* 2T1 cells expressing tetracycline-regulated N- or C-terminal tagged AQP2 (^{3xHA}AQP2 or AQP2^{3xHA}, respectively, in yellow). These proteins localise similar to ISG75 (magenta) at the flagellar pocket/endosomes. The triple *aqp*-null *T. brucei* 2T1 cells (ΔAQP) were also included as control. Scale bar 5 μm. **B)** Tet-regulated expression of N- or C-terminal HA-tagged AQP2. Both native-PAGE (upper panel) and SDS-PAGE (lower panel) αHA blots are shown. α−β tubulin was used as loading control. The presence of the different oligomeric species is indicated in the right-hand side of the panel. Note the presence of a high molecular weight form under SDS-PAGE in ^{3xHA}AQP2 but not AQP2^{3xHA}. The triple *aqp*-null *T. brucei* 2T1 cells (ΔAQP) were also included as control. **C)** EC_{50} values for pentamidine **(left panel)** or salicylhydroxamic acid (SHAM; **right panel**) with or without 5 mM glycerol following expression of either ^{3xHA}AQP2 or AQP2^{3xHA}. For multiparametric ANOVA, we compared the average values (n = 4 independent replicates) from wild type *T. brucei* 2T1 cells as reference for pentamidine, or from *aqp*-null cells for SHAM. * p<0.01, ** p<0.001, *** p<0.0001 from four independent replicates. **D) Left panel;** Representative western blotting (n = 3 independent replicates) from protein turnover

assay monitored by cycloheximide (CHX) treatment in *T. brucei* 2T1 cells expressing either ^{3xHA}AQP2 (upper panel) or AQP2^{3xHA} (lower panel). **Right panel**; Protein quantification from western blotting analysis in left panel for either ^{3xHA}AQP2 (black square) or AQP2^{3xHA} (grey circles). Results are the mean ± standard deviation of three independent experiments (n = 3 independent replicates). The estimated half-life ($t_{1/2}$) was calculated based on regression analysis using PRISM.

Figure 3. TbAQP2 is ubiquitylated in *T. brucei*. A) Cells expressing ^{3xHA}AQP2 were treated with either NH_4^+Cl (10 mM) or MG132 (25 μM) for 1h prior to harvesting. Cell lysates were resolved in a 4-12% acrylamide gel and detected with anti-HA antibody by western blotting. The intensity of anti-β tubulin was used as loading control. **B)** Immunoprecipitation of Δ*aqp* or ^{3xHA}AQP2 cell lysates with anti-HA beads followed by anti-ubiquitin detection by western blotting. An anti-HA blot was also included to confirm protein expression upon induction with tetracycline. Anti-β tubulin was used as loading control. **C)** As in (B), but immunoprecipitation conducted using ubiquitin capture matrix and analysed by western blotting (left panel). The total ("T"), unbound ("Unb."), wash ("W"), and elution ("E") fractions were resolved by SDS-PAGE electrophoresis and analysed with anti-HA immunoblotting (right panel).

Figure 4. TbAQP2 transits through the endosomal compartment and is efficiently delivered and degraded in the lysosome. A) Cell lines expressing a tetracycline-regulated copy of ^{3xHA}AQP2 (Alexa Fluor 488; yellow) were co-stained with anti-TbRab5a and anti-TbRab5b (early endosomes), anti-TbRab11 (recycling endosomes), and anti-p67 (lysosome). All endosomal and lysosomal markers were labelled with secondary antibodies coupled to Alexa Fluor 568 (magenta). DAPI (cyan) was used to label the nucleus and kinetoplast. Scale bars 5 μm. A schematic depiction of the results from confocal microscopy is included in the right panel, generated with BioRender. **B) Left panel**; Protein turnover was monitored by cycloheximide (CHX) treatment. Cells were harvested at various times and the protein level monitored by immunoblotting. ISG75 was included as a control. **Right panel**; Quantification for ISG75 and ^{3xHA}AQP2. Results are the mean ± standard deviation of three independent experiments. **C) Upper panel**; As in (B), but cells were untreated or exposed to 100 nM of bafilomycin A1 (BafA1), or to 25 μM of MG132 for 1 h prior to harvesting. Cell

lysates were resolved by SDS-PAGE followed by western immunoblotting using anti-HA antibody. **Lower panel;** Quantification from three independent experiments - dotted line represents 100% (signal at 0h). Data presented as mean ± standard deviation (n= 3 independent replicates). Statistical analysis was conducted using *t* test; * $p<0.01$ and the signal from untreated cells at 1 h as reference.

Figure 5. N-terminal lysine residues in the N-terminal cytoplasmic tail are important for protein stability, oligomerisation, and anterograde transport. A) Left panel; Structural predictions of ^{3xHA}AQP2 generated with i-Tasser, indicating the three N-terminal lysine residues (magenta) mutated in AQP2$^{3K>R}$. The 3xHA tag has been omitted for simplicity. **Right panel**; Fluorescence microscopy of cells expressing N-terminal HA-tagged wild type AQP2 (AQP2^{WT}) or lysine mutant AQP2$^{3K>R}$. Both proteins are shown in yellow. DAPI (cyan) was used to label the nucleus (N) and the kinetoplast (K). Scale bars, 5 μm. Western blot of cell lysates upon induction with tetracycline are also included. **B)** EC_{50} values for pentamidine (**left panel**) and salicylhydroxamic acid (SHAM) with or without 5 mM glycerol (**right panel**) following recombinant expression of either AQP2^{WT} or AQP2$^{3K>R}$ with a tetracycline-regulated (Tet-on) copy in *T. brucei* 2T1 bloodstream forms. Multiparametric ANOVA calculated as for Figure 4 (N = 3 independent replicates). **C)** Cell lines expressing AQP2^{WT} or AQP2$^{3K>R}$ (Alexa Fluor 488; yellow) were co-stained with anti-BiP (endoplasmic reticulum marker). All markers were labelled with secondary antibodies coupled to Alexa Fluor 568 (magenta). DAPI (cyan) was used to label the nucleus and the kinetoplast, as indicated in (A). Scale bars, 5 μm. **D)** Native-PAGE immunoblot of total cell lysates expressing either AQP2^{WT} or AQP2$^{3K>R}$. Coomassie blue staining of the same fractions was used as loading control. The triple *aqp*-null *T. brucei* 2T1 cells (ΔAQP) were also included as control. **E) Left panel;** Protein turnover monitored as in Figure 4 for AQP2^{WT} or AQP2$^{3K>R}$. Cells were either untreated or treated with 25 μM MG132 for 1 h prior to harvest. Cells were harvested at 0 hours and 2 h post-CHX treatment, and lysates analysed by immunoblotting. α−β tubulin was used as loading control. **Right panel**; Protein quantification representing the mean ± standard deviation (n = 3 independent replicates). Dotted line represents 100% (signal in untreated samples). Statistical analysis was conducted using the signal from untreated cells at 2 h as reference group. ** $p<0.001$, ns = not significant, using a *t* test.

Figure 6. Requirement for cytoplasmic-oriented lysine residues for AQP2 stability and trafficking. A) Cell lines expressing a tetracycline-regulated copy of the constructs mentioned in (A) (Alexa Fluor 488; yellow) were co-stained with either αBiP (ER) or αISG75 (localises to flagellar pocket/endosome), both stained with secondary antibodies coupled to Alexa Fluor 568 (magenta). DAPI (cyan) was used to label the nucleus and the kinetoplast. Scale bars, 5 μm. **B)** Representative western blot (n = 3 independent replicates) of protein turnover monitored by cycloheximide (CHX) treatment followed by pulse-chase of cells expressing the constructs in (A). Cells were either untreated or treated with 25 μM MG132 for 1 h prior to harvest. Cells were harvested at 0 hours and 2 h post-CHX treatment and analysed by immunoblotting. Uninduced controls ("Un.") were also included. **C**) EC_{50} values (average ± standard deviation; n = 3 independent replicates) of pentamidine (upper panel) and salicylhydroxamic acid (SHAM) with or without 5 mM glycerol (lower panel) following recombinant expression of either $AQP2^{WT}$, $AQP2^{5K>R}$, or single arginine-to-lysine AQP2 mutants ($AQP2^{R19K}$, $AQP2^{R45K}$, and $AQP2^{R54K}$). Statistical test for significance was conducted using a pairwise *t* test comparison with uninduced cell lines. * $p<0.01$, ** $p<0.001$, *** $p<0.0001$.

Figure 7. Chimerisation of TbAQP2 leads to mislocalisation, reduction in glycerol transport activity and rapid turnover. A) Cell lines expressing N-terminal HA-tagged TbAQP1, TbAQP2, TbAQP3, field-isolate chimeric AQP2/3 (40AT) or a single TMD mutant ($AQP2^{TMD4}$) (Alexa Fluor 488; yellow) co-stained with anti-ISG75 (magenta). DAPI (cyan) was used to label the nucleus and the kinetoplast. Scale bars 5 μm. Western immunoblotting analysis from lysates of cells expressing these constructs are also included. Anti-β tubulin was used as loading control. **B)** BN-PAGE immunoblot of total cell lysates expressing the constructs in (A). Coomassie blue staining of the same fractions was used as loading control. **C)** EC_{50} values (average ± standard deviation; n = 3) for salicylhydroxamic acid (SHAM) with or without 5 mM glycerol following recombinant expression of the constructs in (A). **D) Left panel**; Representative western blotting (n = 3 independent replicates) analysis of protein turnover monitored by cycloheximide (CHX) treatment followed by pulse-chase of cells expressing the constructs in (A). **Right panel**; Protein quantification representing the mean ± standard deviation of three independent experiments. Dotted line represents

851 50% of protein abundance. Data presented as mean ± standard deviation (n = 3
852 independent replicates).
853
854 **Figure 8. Differential turnover rate of the repertoire of AQPs in the bloodstream**
855 **form of *T. brucei*. A)** Cell lines expressing N-terminal HA-tagged TbAQP1, TbAQP2,
856 TbAQP3, field-isolate chimeric AQP2/3 (40AT) or a single TMD mutant ($AQP2^{TMD4}$)
857 (Alexa Fluor 488; yellow) co-stained with the endoplasmic reticulum marker anti-BiP
858 (magenta). DAPI (cyan) was used to label the nucleus and the kinetoplast. Scale bars,
859 5 μm. **B) Upper panel**; Representative western blot (n = 3 independent replicates) of
860 protein turnover monitored by cycloheximide (CHX) treatment followed by pulse-chase
861 assay. Cells were either untreated or treated with 100 nM of Bafilomycin A1 (BafA1)
862 or 25 μM of MG132 for 1 h prior to harvest. Cells were harvested at 0 hours and 2 h
863 post-CHX treatment and analysed by immunoblotting. **Lowe panel;** Protein
864 quantification representing the mean ± standard deviation of three independent
865 experiments (n = 3 independent replicates). Statistical analysis was conducted using
866 the signal from untreated cells at 2 h post-CHX treatment as reference group. * $p<0.01$,
867 ** $p<0.001$, ns = not significant, using a *t*-test.

868 **Supplementary material for:**

869

870 # Instability of aquaglyceroporin 2 contributes to drug resistance in
871 # *Trypanosoma brucei*

872

873 Juan F. Quintana[1], Juan Bueren-Calabuig[1], Fabio Zuccotto[1], Harry de Koning[2], David
874 Horn[1], and Mark C. Field[1,3]*

875

876 [1]School of Life Sciences, University of Dundee, Dow Street, Dundee DD1 5EH, UK.
877 [2]Institute of Infection, Immunity, and Inflammation, University of Glasgow, Glasgow,
878 UK. [3]Biology Centre, Institute of Parasitology, Biology Centre, Czech Academy of
879 Sciences, Ceske Budejovice, Czech Republic.

880

881

882 ## Supplementary figure legends

883

884 **Figure S1. Characterisation of *T. brucei* 2T1 cell lines expressing N- or C-**
885 **terminal tagged TbAQP2. A)** Proliferation was estimated over a period of four days
886 *in vitro* in the presence or absence of tetracycline for ^{3xHA}AQP2 (middle panel) or
887 AQP2^{3xHA} (right panel) cell lines. *T. brucei* 2T1 wild type *aqp*-null cell lines (left panel)
888 were included as the parental strain. **B)** Dose-response curves for pentamidine from
889 *T. brucei* 2T1 wild type of *aqp*-null cell lines (left panel), ^{3xHA}AQP2 (middle panel), and
890 AQP2^{3xHA} (right panel). **C)** Dose-response curves for SHAM (left panels) or SHAM
891 plus 5 mM glycerol (right panels), with the same lines as in panels A and B.

892

893 **Figure S2. 3xHA C-terminally tagged AQP2 transits through endosomes and is**
894 **delivered into the lysosome.** Cell lines expressing a tetracycline-regulated copy of
895 AQP2^{3xHA} (Alexa Fluor 488; yellow) were co-stained with anti-TbRab5a and anti-
896 TbRab5b (early endosomes), anti-TbRab11 (recycling endosomes) and anti-p67
897 (lysosome). All endosomal and lysosomal markers were labelled with secondary
898 antibodies coupled to Alexa Fluor 568 (magenta). DAPI (cyan) was used to label the
899 nucleus and kinetoplast. Scale bars, 5 μm.

900

Figure S3. Topological predictions of kinetoplastid aquaglyceroporins. TbAQP1, TbAQP2, TbAQP3, a field-isolated chimera AQP2/3 (40AT) and a single TMD mutant ($AQP2^{TMD4}$) are predicted to have both N- and C-termini facing the cytoplasm and six TMD. Predictions were generated using TMHMM (v2.0) [55].

Figure S4. Characterisation of *T. brucei* 2T1 cell lines expressing N-terminal tagged $TbAQP2^{R234K}$ mutant. A) Blue native-PAGE immunoblot of total cell lysates expressing either TbAQP2 ($AQP2^{WT}$), N-terminal lysine-to-arginine mutant ($AQP2^{3K>R}$), all lysine-to-arginine mutant ($AQP2^{5K>R}$) and individual arginine-to-lysine mutants ($AQP2^{R19K}$, $AQP2^{R45K}$, and $AQP2^{R54K}$). Coomassie blue staining of the same lysates was used as loading control. **B)** Blue native-PAGE immunoblot of total cell lysates expressing the constructs in (A). Coomassie blue of the same fractions was used as loading control. **C)** Cell lines expressing a tetracycline-regulated copy of wild type TbAQP2 ($AQP2^{WT}$), N-terminal lysine-to-arginine mutant ($AQP2^{3K>R}$), all lysine-to-arginine mutant ($AQP2^{5K>R}$) or individual arginine-to-lysine mutants ($AQP2^{R234K}$) (Alexa Fluor 488; yellow) were co-stained with anti-TbBiP (endoplasmic reticulum) coupled to Alexa Fluor 568 (magenta). DAPI (cyan) was used to label the nucleus and the kinetoplast. Scale bars 5 μm. **D)** Protein turnover was monitored by cycloheximide (CHX) treatment followed by chase and western blotting. Prior to treatment, cells were either untreated or treated with 25 μM MG132 for 1 hour. Cells were harvested at 0 and 2 hours post-CHX treatment and cell lysates analyses by western immunoblotting. Quantification represents mean ± standard deviation (n = 3 independent replicates), and dotted line represents protein abundance at time 0h. Statistical analysis was conducted using untreated cells at 2 hours as reference group. ** $p<0.001$, *ns* = not significant, using a *t*-test. EC_{50} values for pentamidine **(E)** and salicylhydroxamic acid (SHAM) **(F)** with or without 5 mM glycerol following expression of $AQP2^{R234K}$. Statistical analysis was conducted using untreated cells as reference group. ** $p<0.001$, ns = not significant, using a *t* test. Note that this is an extended version of Figure 6A and 6B, and the full panel included for comparison. **G) Left panel**; View from the cytoplasmic face The TMD4-TMD5 loops in each monomer are highlighted. K234 is shown as spheres. **Right panel**; Structural overview of *T. brucei* AQP2 homology model. K147 and K234 are shown as spheres. The expanded view of the conformational change observed during TMD simulations on TMD1 and TMD3 as a

result of the K147R mutation. Wild type TbAQP2 is shown in green. TbAQP2 displaying the K147R and K234R mutations is shown in light orange.

Figure S5. Protein sequence alignment of wild-type TbAQP2, TbAQP3, and the chimeric AQP2-3 detected in relapsing sleeping sickness patients from the Democratic Republic of Congo. The sequence alignment was conducted using Jalview and MUSCLE for multiple sequence alignment. The NPA/NPS selectivity filter is indicated with red boxes, and predicted *trans*-membrane domain (TMDs) spans are also indicated.

Figure S6. Structural details of TbAQP2 chimerisation and selectivity filters. 3D structural predictions of N-terminal tagged TbAQP1 (cyan), TbAQP2 (magenta), TbAQP3 (green) and the chimeric TbAQP2/3 40AT and AQP2^{TMD4}, with the corresponding domain swap colour-coded. Structures were calculated with i-Tasser. The 3xHA-tag is omitted for simplicity. Details of the selectivity pore for each of these proteins (12Å) are also included. For TbAQP2, AQP2^{TMD4} and 40AT constructs, the selectivity filter is composed of the “NSA/NPS” motif, whereas TbAQP1 and TbAQP3 contain a “NPA/NPA” motif.

Table 1. Summary of the impact of cytoplasmic lysine mutagenesis on TbAQP2 localisation and function.

Protein	Localisation	Protein abundance post-CHX[2]		Proposed degradation pathway	EC_{50} pentamidine (nM)[3]	EC_{50} SHAM (μM)[3]	EC_{50} SHAM + 5 mM glycerol (μM)[3]
		Untreated	+ MG132				
$AQP2^{WT}$	Flagellar pocket	61.05 ± 3.43%	44.42 ± 13.15%	Lysosome	3.29	1.96	1.16
[1]$AQP2^{R19K}$	Endoplasmic reticulum	14.42 ± 9.5%	16.11 ± 7.1%	ERAD[1]	51.18	1.92	1.12
$AQP2^{R45K}$	Endoplasmic reticulum	1.3 ± 0.93%	34.3 ± 4.65%	ERAD	43.16	1.99	2.36
$AQP2^{R54K}$	Endoplasmic reticulum	10.84 ± 0.5%	41.05 ± 12.5%	ERAD	43.10	2.10	2.38
$AQP2^{R234K}$	Endoplasmic reticulum	7.67 ± 1.9%	24.91 ± 5.12%	ERAD	39.95	1.28	2.34
$AQP2^{3K>R}$	Endoplasmic reticulum	5.16 ± 0.62%	46.18 ± 5.95%	ERAD	27.20	10.10	10.14
$AQP2^{5K>R}$	Endoplasmic reticulum	16.8 ± 6.2%	37.5 ± 9.5%	ERAD	41.98	1.34	1.25

[1]$AQP2^{R19K}$ did not show a significant accumulation upon MG132 treatment, but co-localized with TbBiP, indicating probable ERAD-mediated turnover. [2]Protein abundance was calculated 2h post-treatment with cycloheximide (CHX) and expressed as percent of protein abundance compared to protein signal before treatment ("time 0h"). [3]Estimated EC_{50} values from cells induced with tetracycline, 1 μg/ml for 24h.

Table 2. Summary of the impact of chimerisation on TbAQP2 localisation and function.

Protein	Sequence source	Localisation	Half-life (h)	EC_{50} pentamidine (nM)[1]	EC_{50} SHAM (μM)[1]	EC_{50} SHAM + 5 mM glycerol (μM)[1]
TbAQP1	Wild type	Flagellar base	4.34	10.08	3.02	1.45
TbAQP2	Wild type	Flagellar pocket	4.83	3.29	1.96	1.16
TbAQP3	Wild type	Plasma membrane	1.15	10.23	1.28	1.14
40AT	Chimera	Plasma membrane	1.64	10.34	1.39	1.12
$AQP2^{TMD4}$	Chimera	Plasma membrane	<1h	10.24	0.74	0.64

[1]Estimated EC_{50} values from cells induced with tetracycline, 1μg/ml for 24h.

Figure 1

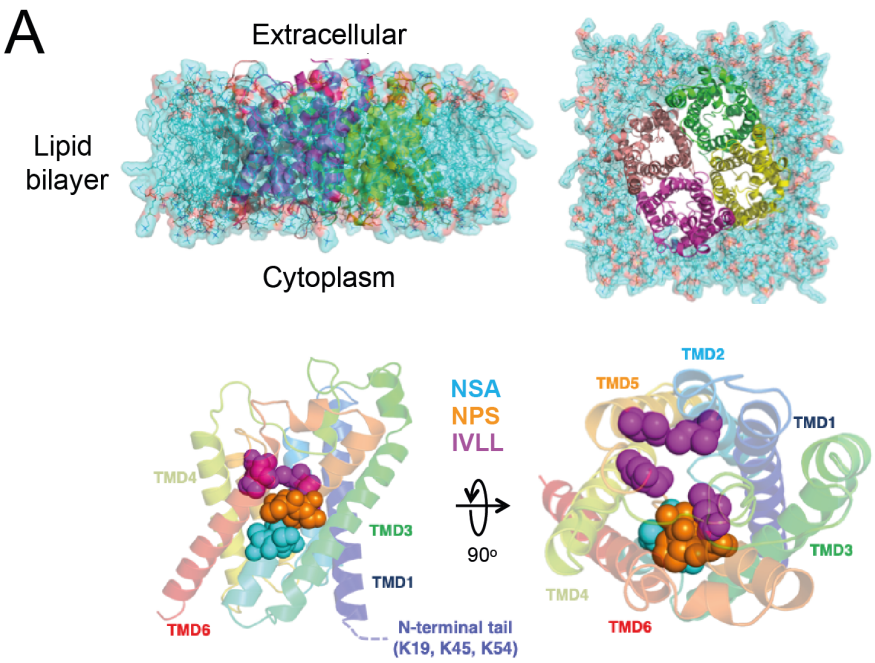

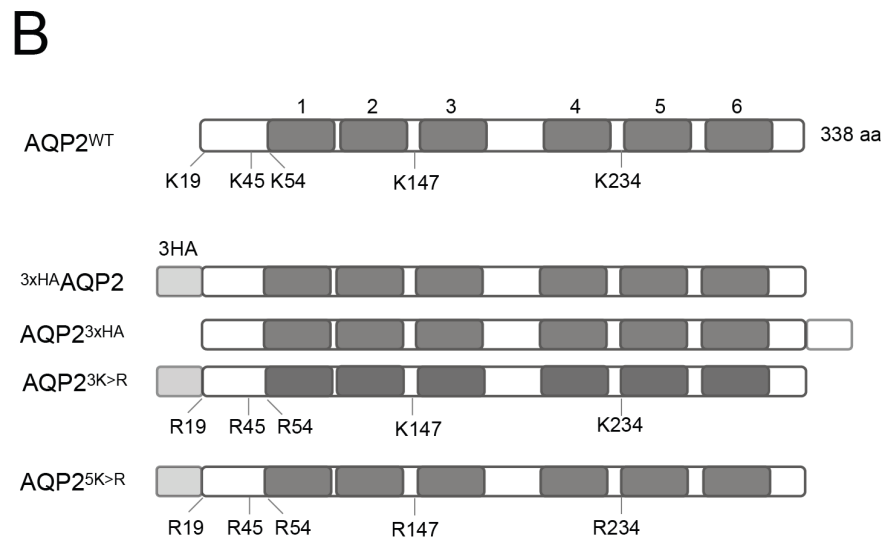

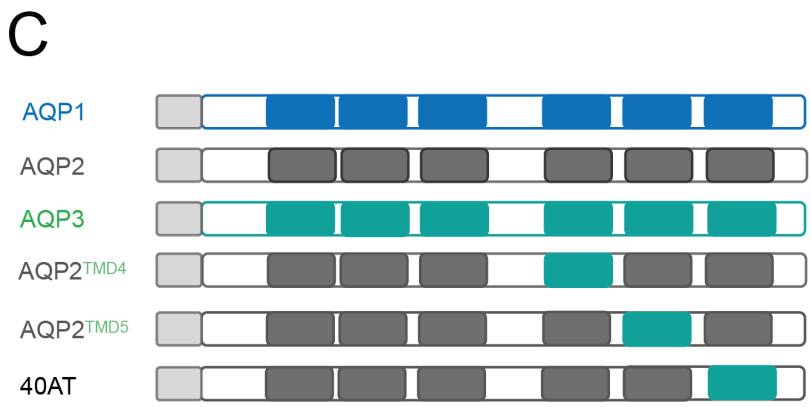

Figure 2

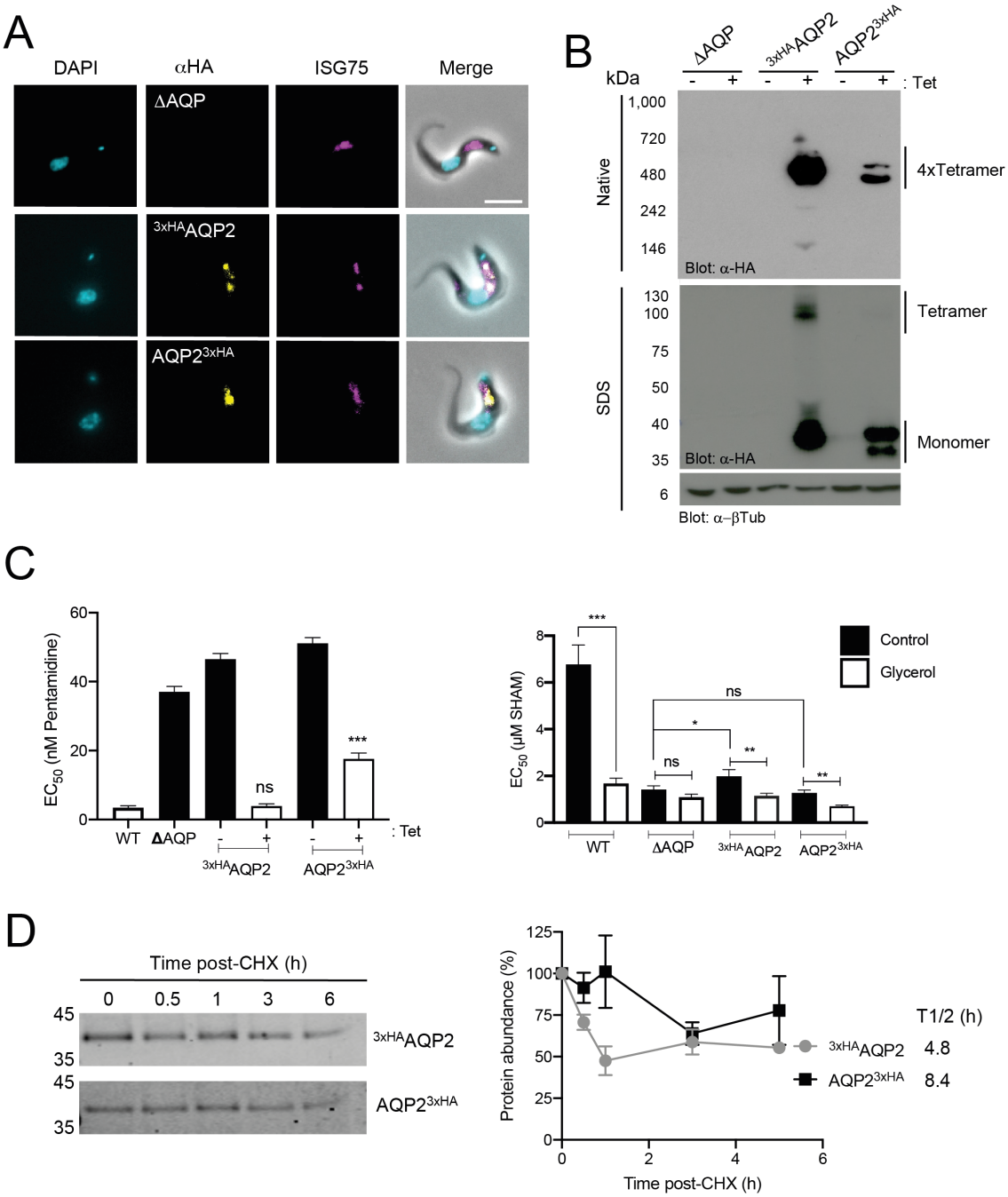

Figure 3

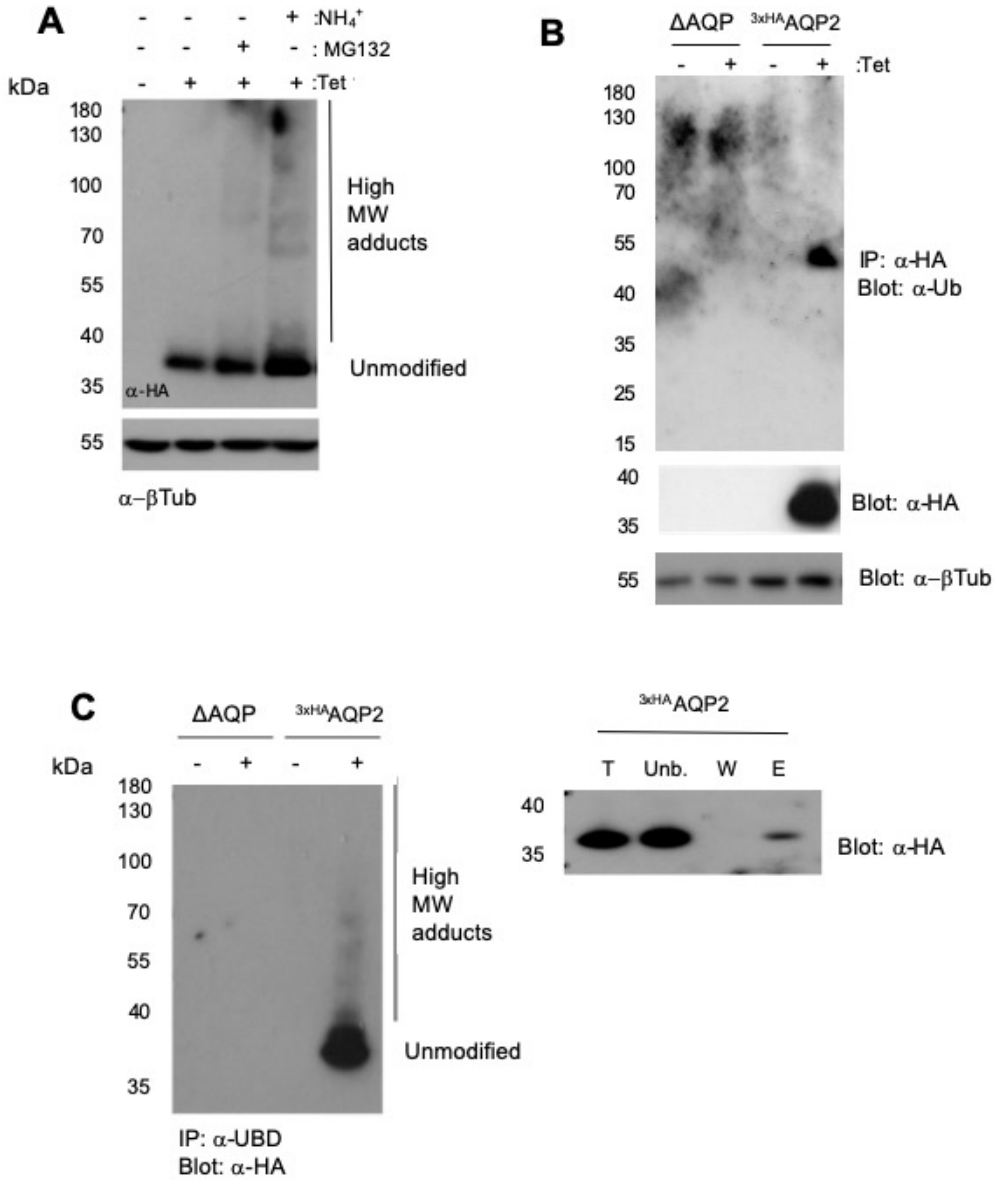

Figure 4

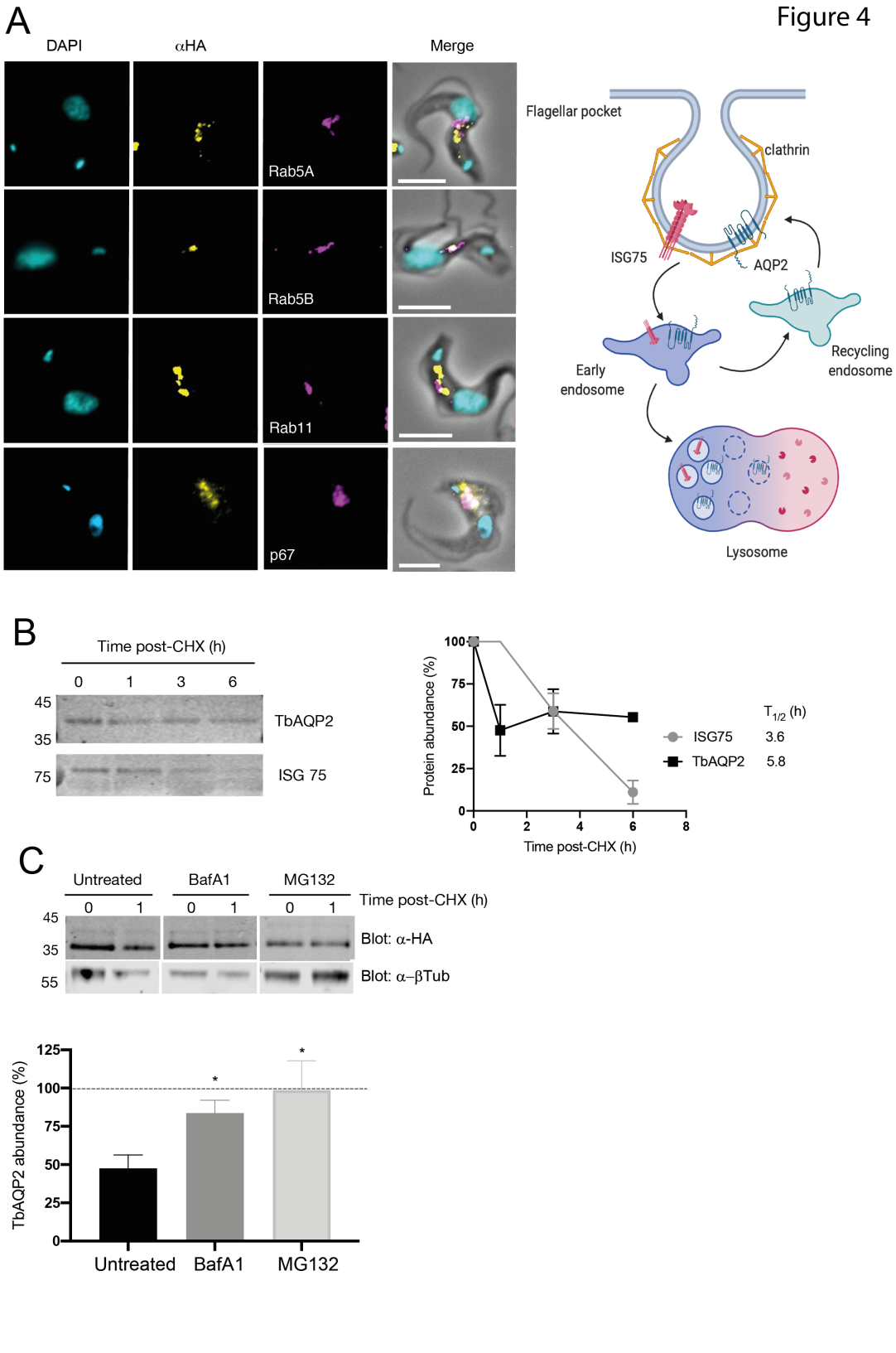

Figure 5

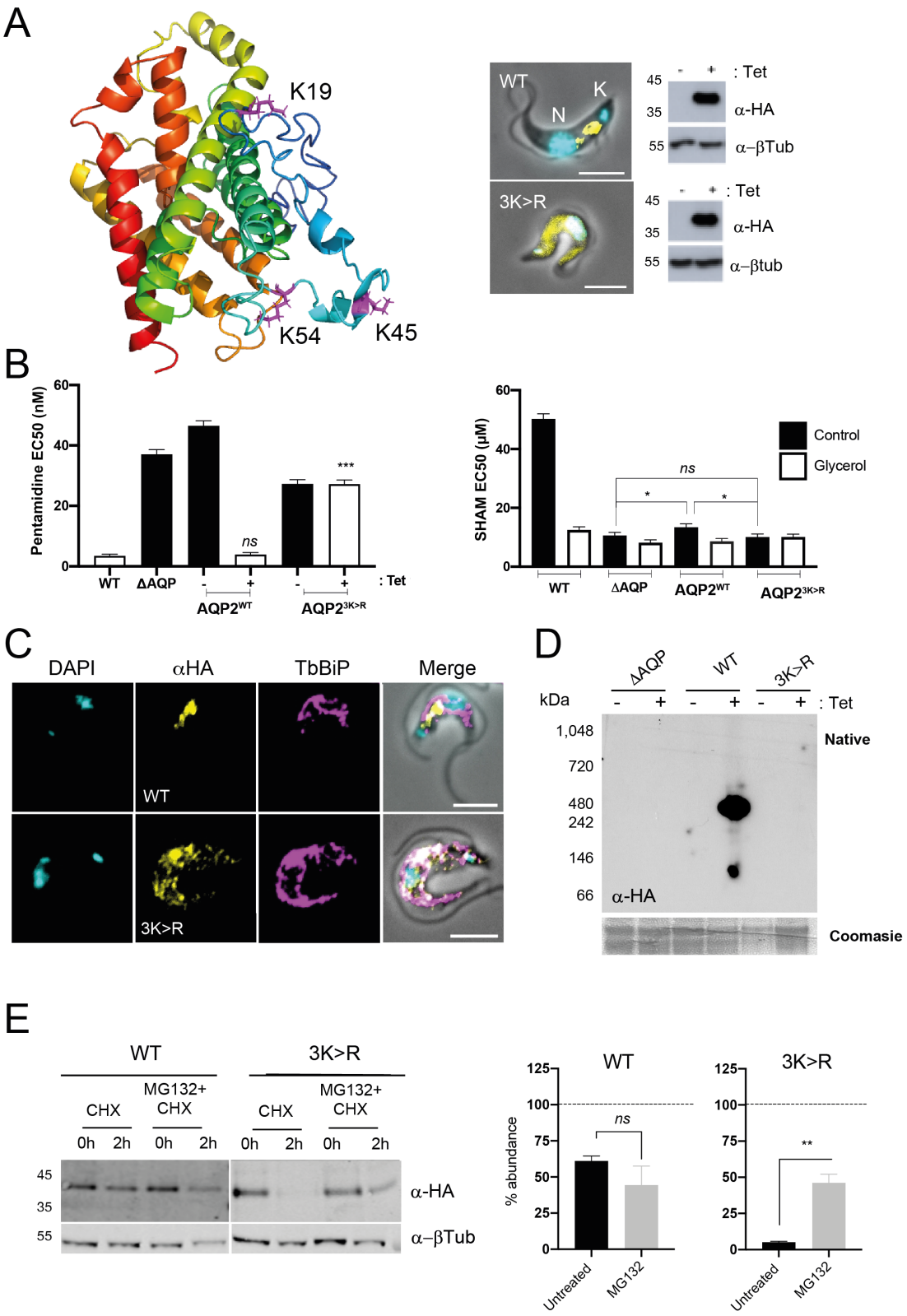

Figure 6

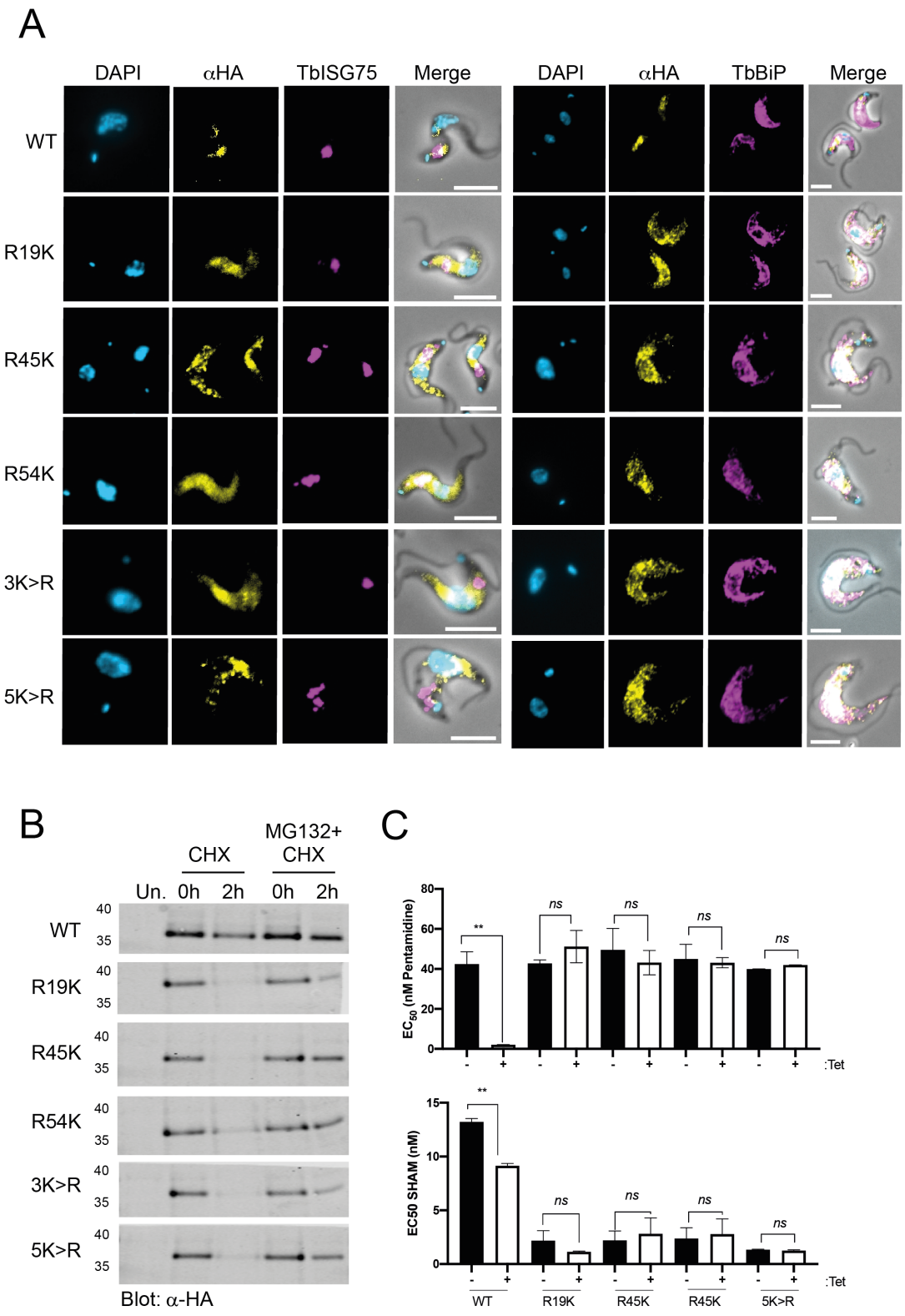

Figure 7

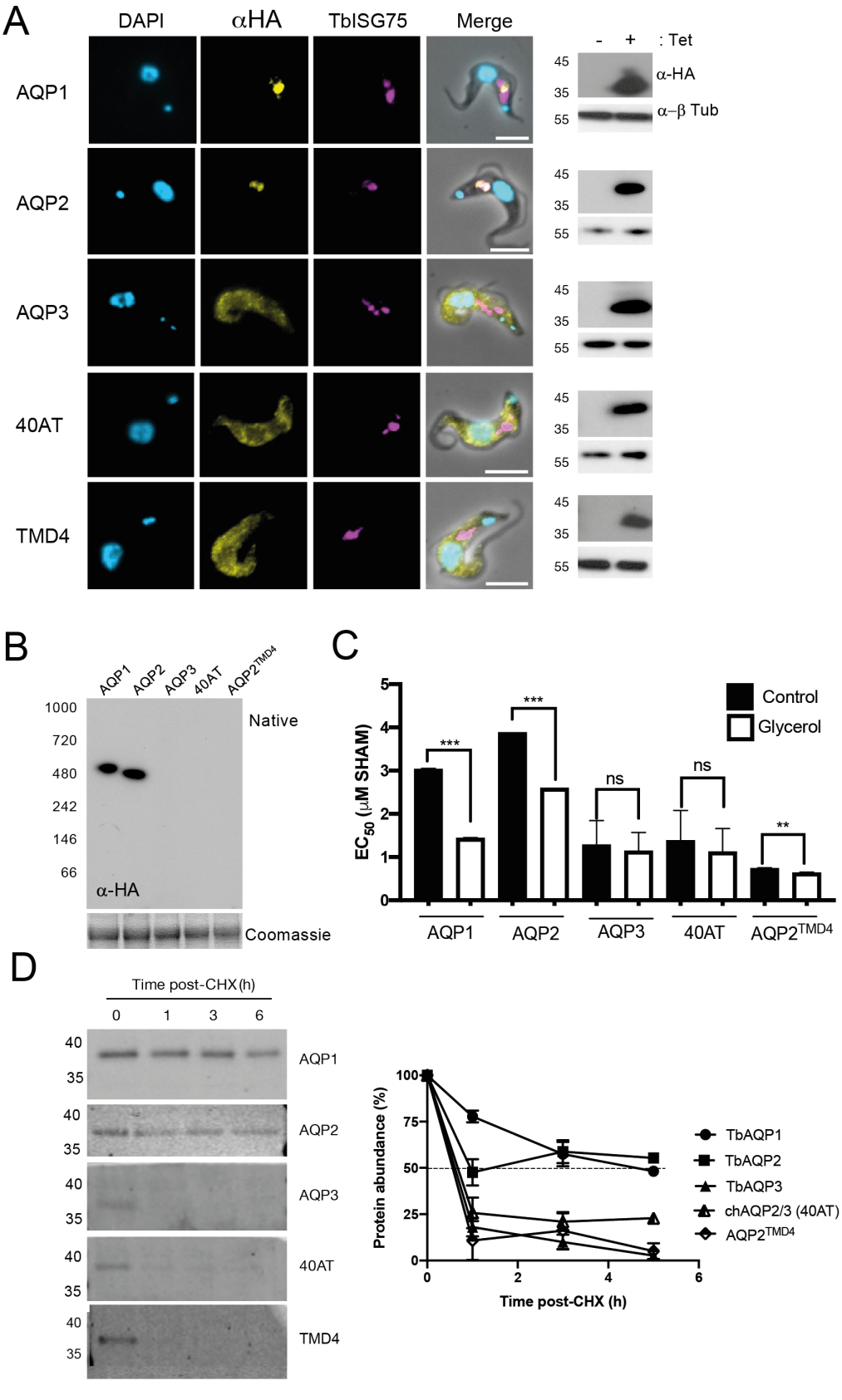

Figure 8

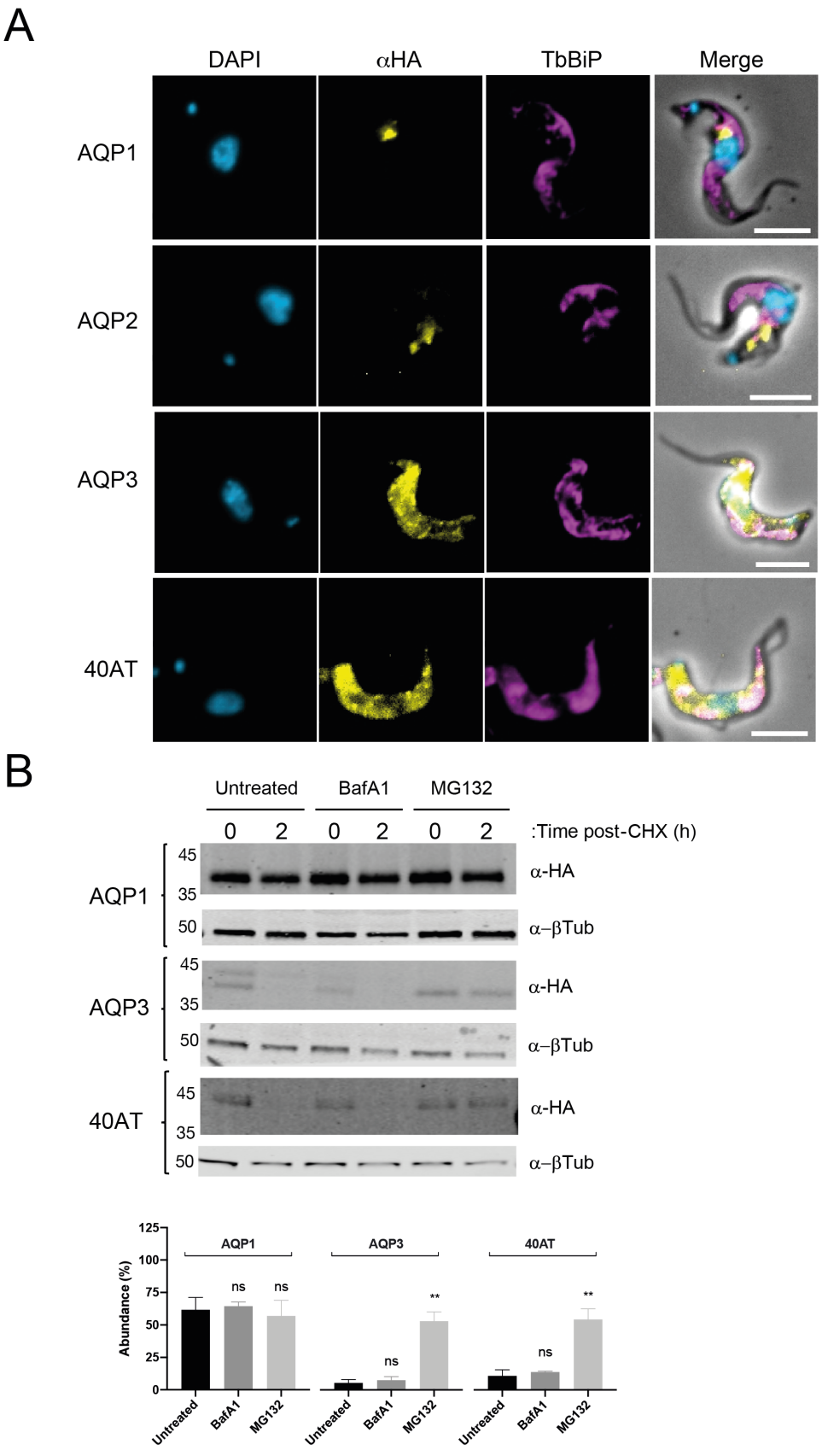

Figure S1

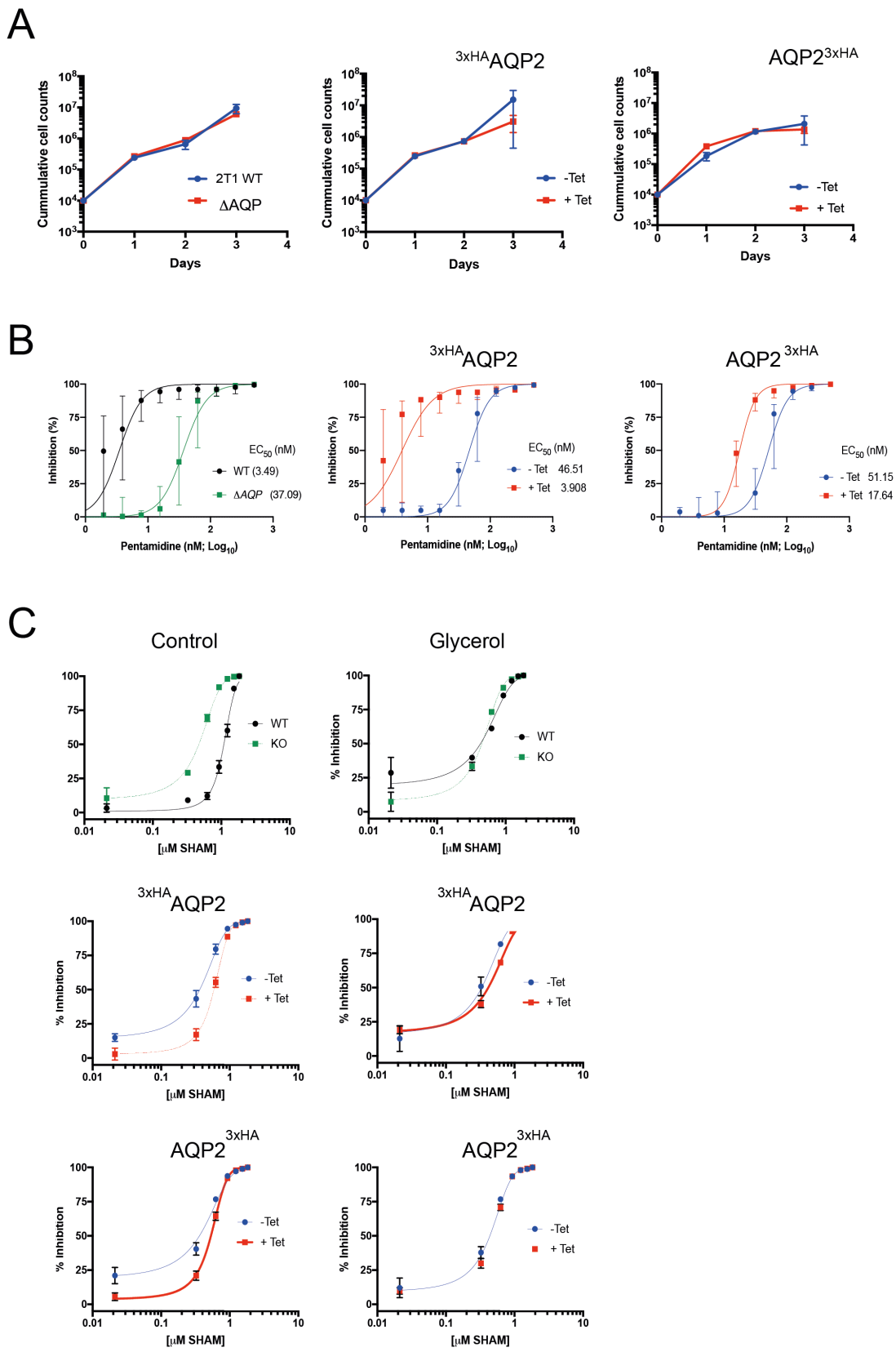

Figure S2

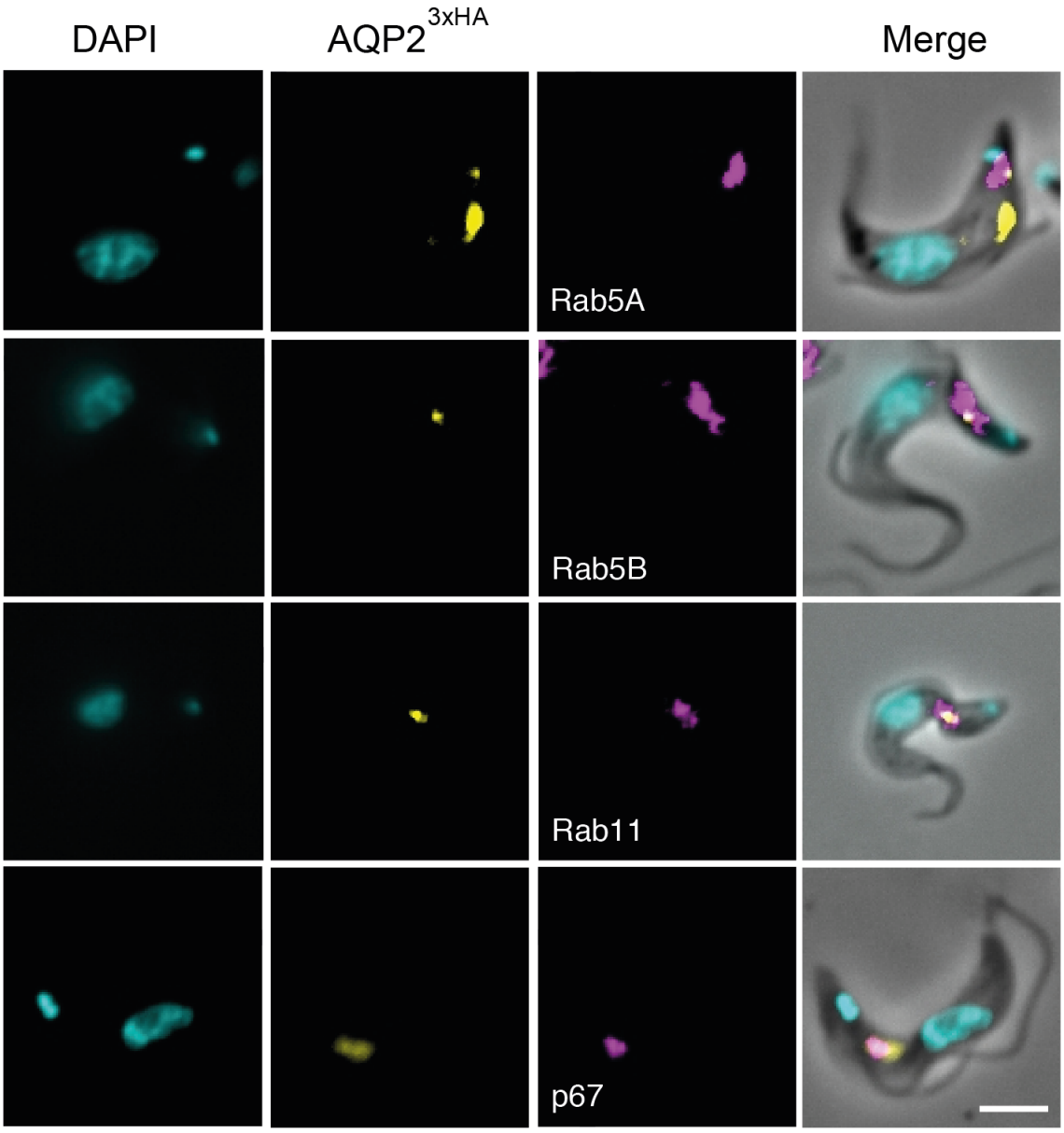

Figure S3

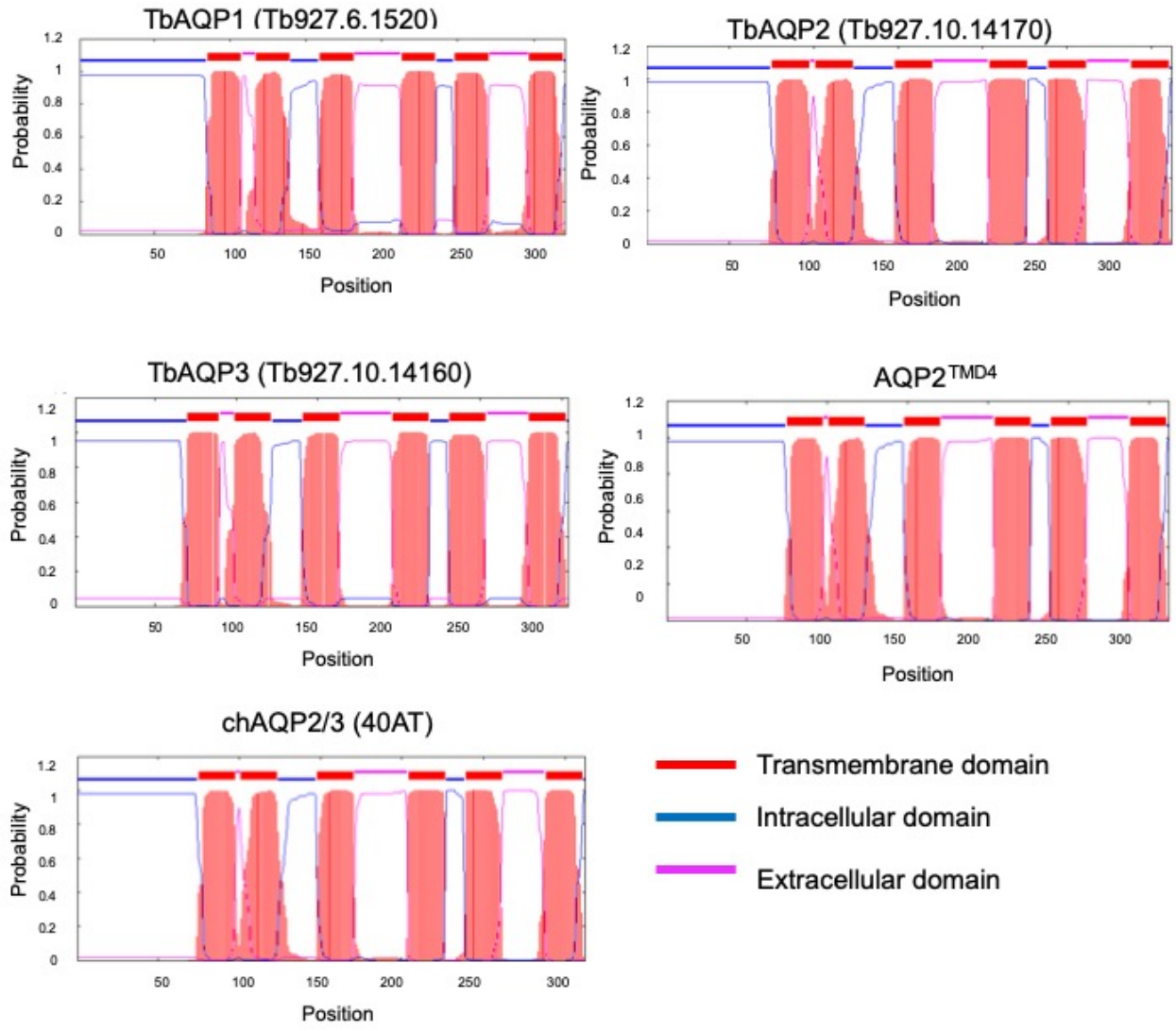

Figure S4

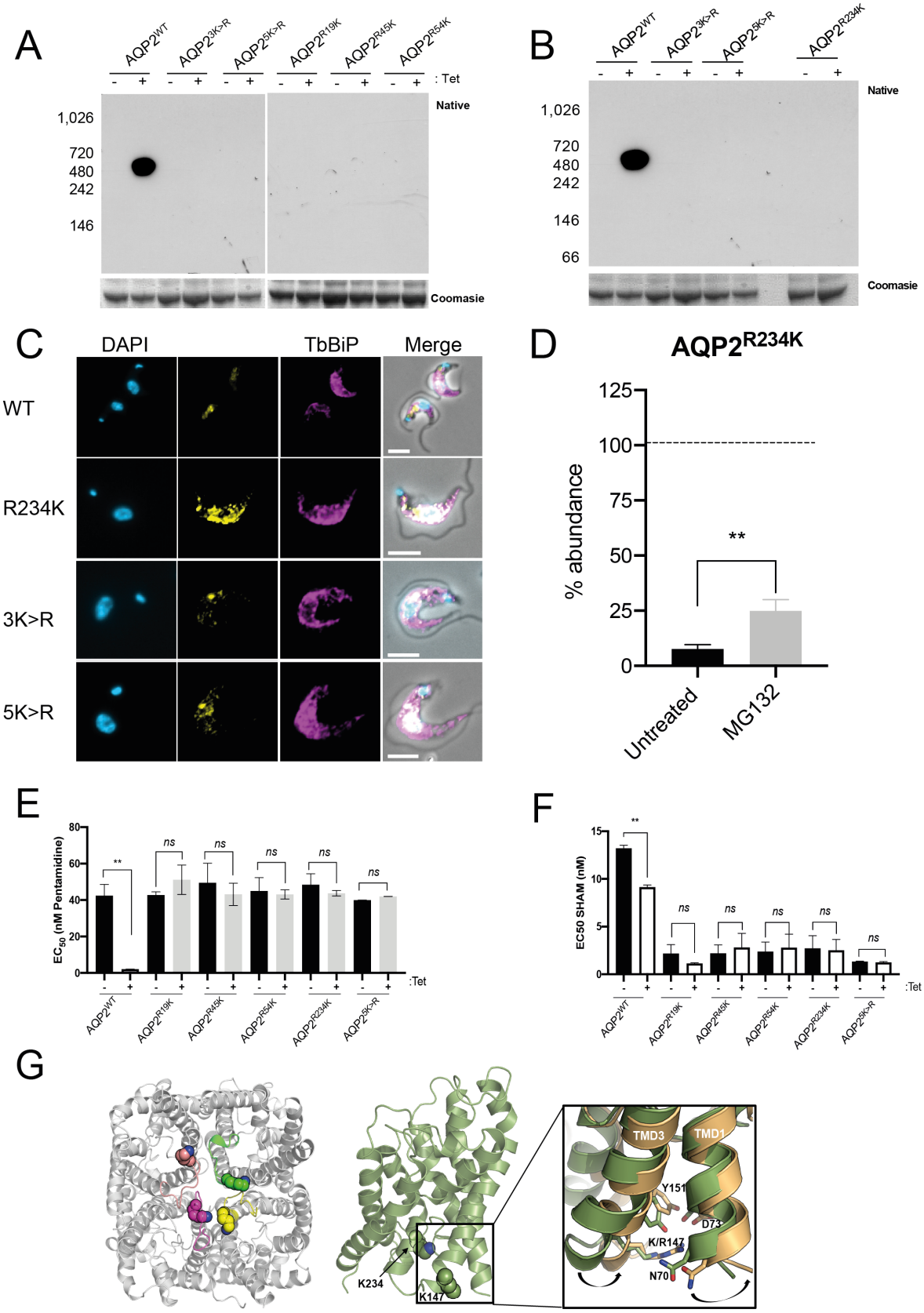

Figure S5

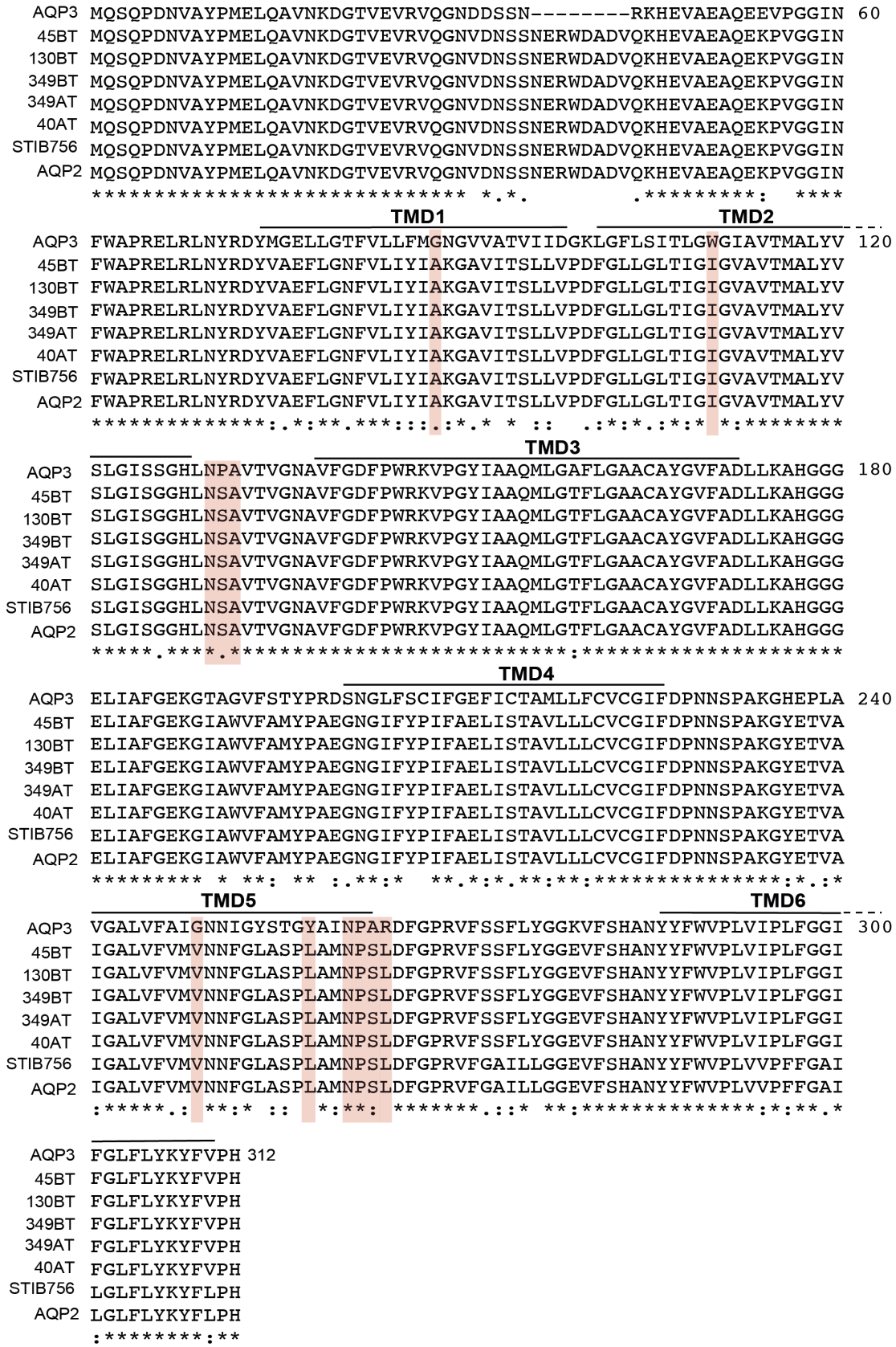

Figure S6